Eur. Phys. J. C 11, 599–618 (1999)
Digital Object Identifier (DOI) 10.1007/s100529900208

THE EUROPEAN PHYSICAL JOURNAL C

Study of τ decays involving kaons, spectral functions and determination of the strange quark mass

The ALEPH Collaboration

R. Barate, D. Decamp, P. Ghez, C. Goy, J.-P. Lees, E. Merle, M.-N. Minard, B. Pietrzyk
Laboratoire de Physique des Particules (LAPP), IN^{2}P^3-CNRS, 74019 Annecy-le-Vieux Cedex, France

R. Alemany, M.P. Casado, M. Chmeissani, J.M. Crespo, E. Fernandez, M. Fernandez-Bosman, Ll. Garrido[15], E. Graugès, A. Juste, M. Martinez, G. Merino, R. Miquel, Ll.M. Mir, A. Pacheco, I.C. Park, I. Riu
Institut de Física d'Altes Energies, Universitat Autònoma de Barcelona, 08193 Bellaterra (Barcelona), Spain[7]

A. Colaleo, D. Creanza, M. de Palma, G. Gelao, G. Iaselli, G. Maggi, M. Maggi, S. Nuzzo, A. Ranieri, G. Raso, F. Ruggieri, G. Selvaggi, L. Silvestris, P. Tempesta, A. Tricomi[3], G. Zito
Dipartimento di Fisica, INFN Sezione di Bari, 70126 Bari, Italy

X. Huang, J. Lin, Q. Ouyang, T. Wang, Y. Xie, R. Xu, S. Xue, J. Zhang, L. Zhang, W. Zhao
Institute of High-Energy Physics, Academia Sinica, Beijing, P.R. China[8]

D. Abbaneo, U. Becker[19], G. Boix[6], M. Cattaneo, V. Ciulli, G. Dissertori, H. Drevermann, R.W. Forty, M. Frank, A.W. Halley, J.B. Hansen, J. Harvey, P. Janot, B. Jost, I. Lehraus, O. Leroy, P. Mato, A. Minten, A. Moutoussi, F. Ranjard, L. Rolandi, D. Rousseau, D. Schlatter, M. Schmitt[20], O. Schneider[23], W. Tejessy, F. Teubert, I.R. Tomalin, E. Tournefier, A.E. Wright
European Laboratory for Particle Physics (CERN), 1211 Geneva 23, Switzerland

Z. Ajaltouni, F. Badaud, G. Chazelle, O. Deschamps, A. Falvard, C. Ferdi, P. Gay, C. Guicheney, P. Henrard, J. Jousset, B. Michel, S. Monteil, J-C. Montret, D. Pallin, P. Perret, F. Podlyski
Laboratoire de Physique Corpusculaire, Université Blaise Pascal, IN^{2}P^3-CNRS, Clermont-Ferrand, 63177 Aubière, France

J.D. Hansen, J.R. Hansen, P.H. Hansen, B.S. Nilsson, B. Rensch, A. Wäänänen
Niels Bohr Institute, 2100 Copenhagen, Denmark[9]

G. Daskalakis, A. Kyriakis, C. Markou, E. Simopoulou, I. Siotis, A. Vayaki
Nuclear Research Center Demokritos (NRCD), 15310 Attiki, Greece

A. Blondel, G. Bonneaud, J.-C. Brient, A. Rougé, M. Rumpf, M. Swynghedauw, M. Verderi, H. Videau
Laboratoire de Physique Nucléaire et des Hautes Energies, Ecole Polytechnique, IN^{2}P^3-CNRS, 91128 Palaiseau Cedex, France

E. Focardi, G. Parrini, K. Zachariadou
Dipartimento di Fisica, Università di Firenze, INFN Sezione di Firenze, 50125 Firenze, Italy

R. Cavanaugh, M. Corden, C. Georgiopoulos
Supercomputer Computations Research Institute, Florida State University, Tallahassee, FL 32306-4052, USA[13,14]

A. Antonelli, G. Bencivenni, G. Bologna[4], F. Bossi, P. Campana, G. Capon, F. Cerutti, V. Chiarella, P. Laurelli, G. Mannocchi[5], F. Murtas, G.P. Murtas, L. Passalacqua, M. Pepe-Altarelli[1]
Laboratori Nazionali dell'INFN (LNF-INFN), 00044 Frascati, Italy

L. Curtis, J.G. Lynch, P. Negus, V. O'Shea, C. Raine, P. Teixeira-Dias, A.S. Thompson
Department of Physics and Astronomy, University of Glasgow, Glasgow G12 8QQ, UK[10]

O. Buchmüller, S. Dhamotharan, C. Geweniger, P. Hanke, G. Hansper, V. Hepp, E.E. Kluge, A. Putzer, J. Sommer, K. Tittel, S. Werner[19], M. Wunsch
Institut für Hochenergiephysik, Universität Heidelberg, 69120 Heidelberg, Germany[16]

R. Beuselinck, D.M. Binnie, W. Cameron, P.J. Dornan[1], M. Girone, S. Goodsir, E.B. Martin, N. Marinelli, J.K. Sedgbeer, P. Spagnolo, E. Thomson, M.D. Williams
Department of Physics, Imperial College, London SW7 2BZ, UK[10]

V.M. Ghete, P. Girtler, E. Kneringer, D. Kuhn, G. Rudolph
Institut für Experimentalphysik, Universität Innsbruck, 6020 Innsbruck, Austria[18]

A.P. Betteridge, C.K. Bowdery, P.G. Buck, P. Colrain, G. Crawford, A.J. Finch, F. Foster, G. Hughes, R.W.L. Jones, N.A. Robertson, M.I. Williams
Department of Physics, University of Lancaster, Lancaster LA1 4YB, UK[10]

I. Giehl, C. Hoffmann, K. Jakobs, K. Kleinknecht, G. Quast, B. Renk, E. Rohne, H.-G. Sander, P. van Gemmeren, H. Wachsmuth, C. Zeitnitz
Institut für Physik, Universität Mainz, 55099 Mainz, Germany[16]

J.J. Aubert, C. Benchouk, A. Bonissent, J. Carr[1], P. Coyle, F. Etienne, F. Motsch, P. Payre, M. Talby, M. Thulasidas
Centre de Physique des Particules, Faculté des Sciences de Luminy, IN^{2}P^3-CNRS, 13288 Marseille, France

M. Aleppo, M. Antonelli, F. Ragusa
Dipartimento di Fisica, Università di Milano e INFN Sezione di Milano, 20133 Milano, Italy

R. Berlich, V. Büscher, H. Dietl, G. Ganis, K. Hüttmann, G. Lütjens, C. Mannert, W. Männer, H.-G. Moser, S. Schael, R. Settles, H. Seywerd, H. Stenzel, W. Wiedenmann, G. Wolf
Max-Planck-Institut für Physik, Werner-Heisenberg-Institut, 80805 München, Germany[p]

P. Azzurri, J. Boucrot, O. Callot, S. Chen, A. Cordier, M. Davier, L. Duflot, J.-F. Grivaz, Ph. Heusse, A. Höcker, A. Jacholkowska, D.W. Kim[12], F. Le Diberder, J. Lefrançois, A.-M. Lutz, M.-H. Schune, J.-J. Veillet, I. Videau[1], D. Zerwas
Laboratoire de l'Accélérateur Linéaire, Université de Paris-Sud, IN^{2}P^3-CNRS, 91898 Orsay Cedex, France

G. Bagliesi, S. Bettarini, T. Boccali, C. Bozzi[24], G. Calderini, R. Dell'Orso, I. Ferrante, L. Foà, A. Giassi, A. Gregorio, F. Ligabue, A. Lusiani, P.S. Marrocchesi, A. Messineo, F. Palla, G. Rizzo, G. Sanguinetti, A. Sciabà, G. Sguazzoni, R. Tenchini, C. Vannini, A. Venturi, P.G. Verdini
Dipartimento di Fisica dell'Università, INFN Sezione di Pisa, e Scuola Normale Superiore, 56010 Pisa, Italy

G.A. Blair, G. Cowan, M.G. Green, T. Medcalf, J.A. Strong, J.H. von Wimmersperg-Toeller
Department of Physics, Royal Holloway & Bedford New College, University of London, Surrey TW20 OEX, UK[10]

D.R. Botterill, R.W. Clifft, T.R. Edgecock, P.R. Norton, J.C. Thompson
Particle Physics Dept., Rutherford Appleton Laboratory, Chilton, Didcot, Oxon OX11 OQX, UK[10]

B. Bloch-Devaux, P. Colas, S. Emery, W. Kozanecki, E. Lançon, M.-C. Lemaire, E. Locci, P. Perez, J. Rander, J.-F. Renardy, A. Roussarie, J.-P. Schuller, J. Schwindling, A. Trabelsi[21], B. Vallage
CEA, DAPNIA/Service de Physique des Particules, CE-Saclay, 91191 Gif-sur-Yvette Cedex, France[17]

S.N. Black, J.H. Dann, R.P. Johnson, H.Y. Kim, N. Konstantinidis, A.M. Litke, M.A. McNeil, G. Taylor
Institute for Particle Physics, University of California at Santa Cruz, Santa Cruz, CA 95064, USA[22]

C.N. Booth, S. Cartwright, F. Combley, M.S. Kelly, M. Lehto, L.F. Thompson
Department of Physics, University of Sheffield, Sheffield S3 7RH, UK[10]

K. Affholderbach, A. Böhrer, S. Brandt, C. Grupen, G. Prange
Fachbereich Physik, Universität Siegen, 57068 Siegen, Germany[16]

G. Giannini, B. Gobbo
Dipartimento di Fisica, Università di Trieste e INFN Sezione di Trieste, 34127 Trieste, Italy

J. Rothberg, S. Wasserbaech
Experimental Elementary Particle Physics, University of Washington, WA 98195 Seattle, USA

S.R. Armstrong, E. Charles, P. Elmer, D.P.S. Ferguson, Y. Gao, S. González, T.C. Greening, O.J. Hayes, H. Hu, S. Jin, P.A. McNamara III, J.M. Nachtman[2], J. Nielsen, W. Orejudos, Y.B. Pan, Y. Saadi, I.J. Scott, J. Walsh, Sau Lan Wu, X. Wu, G. Zobernig
Department of Physics, University of Wisconsin, Madison, WI 53706, USA[11]

[1] Also at CERN, 1211 Geneva 23, Switzerland
[2] Now at University of California at Los Angeles (UCLA), Los Angeles, CA 90024, USA
[3] Also at Dipartimento di Fisica, INFN, Sezione di Catania, 95129 Catania, Italy
[4] Also Istituto di Fisica Generale, Università di Torino, 10125 Torino, Italy
[5] Also Istituto di Cosmo-Geofisica del C.N.R., Torino, Italy
[6] Supported by the Commission of the European Communities, contract ERBFMBICT982894
[7] Supported by CICYT, Spain

[8] Supported by the National Science Foundation of China
[9] Supported by the Danish Natural Science Research Council
[10] Supported by the UK Particle Physics and Astronomy Research Council
[11] Supported by the US Department of Energy, grant DE-FG0295-ER40896
[12] Permanent address: Kangnung National University, Kangnung, Korea
[13] Supported by the US Department of Energy, contract DE-FG05-92ER40742
[14] Supported by the US Department of Energy, contract DE-FC05-85ER250000
[15] Permanent address: Universitat de Barcelona, 08208 Barcelona, Spain
[16] Supported by the Bundesministerium für Bildung, Wissenschaft, Forschung und Technologie, Germany
[17] Supported by the Direction des Sciences de la Matière, C.E.A
[18] Supported by Fonds zur Förderung der wissenschaftlichen Forschung, Austria
[19] Now at SAP AG, 69185 Walldorf, Germany
[20] Now at Harvard University, Cambridge, MA 02138, USA
[21] Now at Département de Physique, Faculté des Sciences de Tunis, 1060 Le Belvédère, Tunisia
[22] Supported by the US Department of Energy, grant DE-FG03-92ER40689
[23] Now at Université de Lausanne, 1015 Lausanne, Switzerland
[24] Now at INFN Sezione de Ferrara, 44100 Ferrara, Italy

Received: 24 February 1999 / Published online: 14 October 1999

Abstract. All ALEPH measurements of branching ratios of τ decays involving kaons are summarized including a combination of results obtained with K^0_S and K^0_L detection. The decay dynamics are studied, leading to the determination of contributions from vector $K^*(892)$ and $K^*(1410)$, and axial-vector $K_1(1270)$ and $K_1(1400)$ resonances. Agreement with isospin symmetry is observed among the different final states. Under the hypothesis of the conserved vector current, the spectral function for the $K\overline{K}\pi$ mode is compared with the corresponding cross section for low energy e^+e^- annihilation, yielding an axial-vector fraction of $(94^{+6}_{-8})\%$ for this mode. The branching ratio for τ decay into all strange final states is determined to be $B(\tau^- \to X^-(S=-1)\nu_\tau) = (28.7 \pm 1.2) \times 10^{-3}$. The measured mass spectra of the strange τ decay modes are exploited to derive the $S=-1$ spectral function. A combination of strange and nonstrange spectral functions is used to determine the strange quark mass and nonperturbative contributions to the strange hadronic width. A method is developed to avoid the bad convergence of the spin zero hadronic component, with the result $m_s(M^2_\tau) = (176^{+46}_{-57})$ MeV/c^2. The evolution down to 1 GeV gives $m_s(1\ \mathrm{GeV}^2) = (234^{+61}_{-76})$ MeV/c^2.

1 Introduction

Hadronic τ decays provide a clean environment for studying the physics of hadrons, which are produced via W exchange, *i.e.*, from the QCD vacuum. For this reason, the global properties of hadronic systems in τ decay are described by fundamental quantities, called spectral functions, which measure the transition probability to create hadrons out of the vacuum as a function of the hadronic mass. Due to their unambiguous theoretical and experimental definition, τ spectral functions provide information on hadron dynamics in an interesting mass region which is dominated by resonances and leads to the simpler asymptotic QCD regime. The ALEPH Collaboration has already published analyses of the nonstrange vector [1] and axial-vector [2] spectral functions. The nonstrange vector spectral function can be compared to the corresponding cross sections in e^+e^- annihilation [1] in order to test isospin invariance of the electroweak vector current, formerly called the conserved vector current (CVC) hypothesis. Detailed QCD studies have been performed using the nonstrange vector and axial-vector spectral functions, resulting in a precise determination of the strong coupling constant $\alpha_s(M_\tau^2)$ [2]. In this paper, attention is turned to the τ decays involving kaons, which are of importance in order to address issues in both strange and nonstrange decay dynamics [3,4].

Recently, ALEPH completed the measurement of τ decay branching ratios involving kaons [5–8], as summarized in Table 1, which allows a comprehensive study of the strange sector and of some aspects of the dynamics in the final states with a $K\overline{K}$ pair. These analyses involve the detection of charged kaons and neutral kaons (K_L^0, K_S^0). Assuming CP invariance the K_S^0 and K_L^0 branching ratios can be averaged. The corresponding results are given in the right-hand column of Table 1. Although the strange final states are Cabibbo suppressed, the precision achieved in these measurements enables many significant tests, ranging from $\mu - \tau$ lepton universality to hadron dynamics, resonance production and QCD analyses. In addition, the results are checked for consistency with isospin relations between the rates observed for different final states.

One of the outstanding issues in the nonstrange sector is the vector and axial-vector composition of the $K\overline{K}\pi$ final state. This was a limitation in the QCD analysis of [2]. New information on this point is obtained from the ALEPH measurement of all relevant decay modes[1] $K_S^0K_L^0\pi^-$, $K_S^0K_S^0\pi^-$, $K^+K^-\pi^-$ and $K^0K^-\pi^0$. In addi-

[1] Throughout this paper, charge conjugate states are implied

Table 1. Summary of branching ratios for τ decays involving kaons from ALEPH data. Channels with neutral kaons are measured separately using their K^0_L and K^0_S components. Modes are split into the strange ($S = -1$) and nonstrange ($S = 0$) sectors of τ decays. Due to the limitations of statistics and particle identification, the net strangeness of the $K^0h^-h^+h^-$ mode has not been determined (h stands for π or K). The last column presents the average of K^0_S and K^0_L results for final states with $\overline{K^0}$ and K^-K^0, and the sum of all components for final states with $K^0\overline{K^0}$

Decay	K^0 detected	S	B (10^{-3})	$B(K^0_L + K^0_S)$ (10^{-3})
$\tau^- \to K^-\nu_\tau$	–		6.96 ± 0.29	–
$\tau^- \to K^-\pi^0\nu_\tau$	–		4.44 ± 0.35	–
$\tau^- \to \overline{K^0}\pi^-\nu_\tau$	K^0_L		9.28 ± 0.56	9.17 ± 0.52
$\tau^- \to \overline{K^0}\pi^-\nu_\tau$	K^0_S		8.55 ± 1.34	
$\tau^- \to \overline{K^0}\pi^-\pi^0\nu_\tau$	K^0_L		3.47 ± 0.65	3.27 ± 0.51
$\tau^- \to \overline{K^0}\pi^-\pi^0\nu_\tau$	K^0_S		2.94 ± 0.82	
$\tau^- \to K^-\pi^+\pi^-\nu_\tau$	–	-1	2.14 ± 0.47	–
$\tau^- \to K^-\pi^0\pi^0\nu_\tau$	–		0.56 ± 0.25	–
$\tau^- \to \overline{K^0}\pi^-\pi^0\pi^0\nu_\tau$	K^0_L		< 0.66 (95% C.L.)	0.26 ± 0.24
$\tau^- \to \overline{K^0}\pi^-\pi^0\pi^0\nu_\tau$	K^0_S		0.58 ± 0.36	
$\tau^- \to K^-\pi^0\pi^0\pi^0\nu_\tau$	–		0.37 ± 0.24 (excl. η)	–
$\tau^- \to K^-\pi^+\pi^-\pi^0\nu_\tau$	–		0.54 ± 0.43 (excl. η)	–
$\tau^- \to K^-\eta\nu_\tau$	–		$0.29^{+0.15}_{-0.14}$	–
$\tau^- \to K^-K^+K^-\nu_\tau$	–		< 0.19 (95% C.L.)	–
$\tau^- \to K^-K^0\nu_\tau$	K^0_L		1.62 ± 0.24	1.61 ± 0.21
$\tau^- \to K^-K^0\nu_\tau$	K^0_S		1.58 ± 0.45	
$\tau^- \to K^-K^0\pi^0\nu_\tau$	K^0_L		1.43 ± 0.29	1.45 ± 0.27
$\tau^- \to K^-K^0\pi^0\nu_\tau$	K^0_S		1.52 ± 0.79	
$\tau^- \to K^-K^0\pi^0\pi^0\nu_\tau$	K^0_L		< 0.18 (95% C.L.)	< 0.16 (95% C.L.)
$\tau^- \to K^-K^0\pi^0\pi^0\nu_\tau$	K^0_S	0	< 0.39 (95% C.L.)	
$\tau^- \to K^0_SK^0_L\pi^-\nu_\tau$	–		1.01 ± 0.26	1.53 ± 0.35
$\tau^- \to K^0_SK^0_S\pi^-\nu_\tau$	–		0.26 ± 0.12	
$\tau^- \to K^0_SK^0_L\pi^-\pi^0\nu_\tau$	–		0.31 ± 0.12	0.31 ± 0.23
$\tau^- \to K^0_SK^0_S\pi^-\pi^0\nu_\tau$	–		< 0.20 (95% C.L.)	
$\tau^- \to K^-K^+\pi^-\nu_\tau$	–		1.63 ± 0.27	–
$\tau^- \to K^-K^+\pi^-\pi^0\nu_\tau$	–		0.75 ± 0.33	–
$\tau^- \to K^0h^-h^+h^-\nu_\tau$	K^0_S	mixed	0.23 ± 0.20	0.23 ± 0.20

tion, the availability of the corresponding isovector cross section measured in e^+e^- annihilation and assuming CVC allows an independent determination of the vector fraction in the $(K\overline{K}\pi)^-\nu_\tau$ channel, with a significant improvement in accuracy.

Because G-parity cannot be defined for the strange hadronic states, it is difficult to separate vector and axial-vector contributions. Furthermore, the relatively low statistics do not permit different spin-parity states to be unfolded from the overall decay distributions. Experimentally, the $\overline{K}\pi\pi$ system is the most complex one to deal with, since it contains contributions from two axial-vector mesons, $K_1(1270)$ and $K_1(1400)$, and one vector meson, $K^*(1410)$. However, the $K^*(1410)$ state can be measured in the $(\overline{K}\pi)^-\nu_\tau$ channel by its interference with the dominant $K^*(892)$ production, analogously to the $\rho(770) - \rho(1450)$ situation in the $\pi\pi^0$ final states [1]. Unlike the $K_1(1400)$ and $K^*(1410)$, the axial-vector $K_1(1270)$ decays significantly into $K\rho$. And so fits to the invariant $\pi\pi$ mass distributions [5–7], which measure the $\overline{K}\rho$ fraction, determine the total $K_1(1270)$ contribution. A fit to the invariant $\overline{K}\pi\pi$ mass spectrum provides additional information on the resonance content. It is important to separate the vector and axial-vector contributions in the strange sector of τ decays to obtain information on the size of the non-perturbative QCD part in the τ hadronic width. This has been observed to be very small in the nonstrange case [2].

Independently of the resonance structure, the total strange spectral function is determined, without separating vector and axial-vector contributions. Similar to the nonstrange sector, the τ strange spectral functions are key ingredients for QCD studies and provide the possibility to follow the results as a function of a variable "τ mass" [2].

One of the free parameters of the Standard Model, the strange quark mass m_s, appears in many phenomenological calculations, such as in the prediction of the CP-violating kaon parameters ϵ'/ϵ [9]. The strange τ decay rate is sensitive to m_s [10] which can be experimentally determined. A breaking of chiral symmetry, induced by the relatively large strange quark mass, introduces a mass dependence into the perturbative QCD prediction of the total strange hadronic width of the τ. Using the total rates and moments of the respective spectral functions, a combination of strange and nonstrange modes can be found which cancels the dominant massless perturbative contribution, enabling the strange quark mass to be derived by means of a combined fit with nonperturbative contributions. An error in the theoretical calculation [11] of the second-order perturbative term was recently pointed out [12]. After correction, a problematic convergence behaviour of the perturbative series is observed [12–14], leading to a larger theoretical uncertainty on m_s than had previously been assumed and to a bias in the central value obtained [3]. In this analysis, particular attention is devoted to this question and a new method is introduced [15] to avoid the convergence problem.

2 $\mu - \tau$ lepton universality

Lepton universality requires that the W^- boson coupling to any lepton pair $l\bar{\nu}_l$ be of the same strength g_l; this hypothesis is in agreement with studies in the leptonic and hadronic sectors [16]. Lepton universality can be tested in the strange sector by comparing the decay widths of $\tau^- \to K^-\nu_\tau$ and $K^- \to \mu^-\bar{\nu}_\mu$. The following ratio, in which the common CKM matrix element and the decay constant f_K both cancel, is precisely predicted by theory:

$$\begin{aligned} R_{\tau/K} &\equiv \frac{\Gamma(\tau^- \to K^-\nu_\tau)}{\Gamma(K^- \to \mu^-\bar{\nu}_\mu)} \\ &\equiv \frac{B(\tau^- \to K^-\nu_\tau)\tau_K}{B(K^- \to \mu^-\bar{\nu}_\mu)\tau_\tau} \\ &= \frac{1}{2}\frac{g_\tau^2}{g_\mu^2}\frac{M_\tau^3}{M_K M_\mu^2}\frac{(1-M_K^2/M_\tau^2)^2}{(1-M_\mu^2/M_K^2)^2}(1+\delta R_{\tau/K}) \ , \end{aligned} \quad (1)$$

with the radiative correction $\delta R_{\tau/K} = (0.90 \pm 0.22)\%$ [17], $B(K^- \to \mu^-\nu_\tau) = B_K = (63.51 \pm 0.18)\%$, $\tau_K = (1.2386 \pm 0.0024) \times 10^{-8}$ s, and $\tau_\tau = (290 \pm 1.2) \times 10^{-15}$ s [18]. Assuming $\mu - \tau$ universality ($g_\tau = g_\mu$), (1) predicts

$$\begin{aligned} B(\tau^- \to K^-\nu_\tau) = (7.14 \pm 0.02_{th} \pm 0.02_{B_K} \pm 0.03_{\tau_\tau}) \\ \times 10^{-3} \ , \end{aligned} \quad (2)$$

where only sizeable contributions to the errors are given (the theoretical uncertainty is from radiative corrections).

The comparison of (2) with the ALEPH measurement

$$B(\tau^- \to K^-\nu_\tau) = (6.96 \pm 0.25 \pm 0.14) \times 10^{-3} \quad (3)$$

yields

$$g_\tau/g_\mu = 0.987 \pm 0.021, \quad (4)$$

which agrees with the universality assumption within one standard deviation.

The measurement (3) can also be exploited to determine f_K if lepton universality is assumed to hold. One obtains[2]

$$\begin{aligned} f_K = \frac{1}{G_F|V_{us}|}\left(1 - \frac{M_K^2}{M_\tau^2}\right)^{-1} \\ \times M_\tau^{-\frac{3}{2}}\sqrt{\frac{B(\tau^- \to K^-\nu_\tau)}{\tau_\tau}} \ , \end{aligned} \quad (5)$$

where $G_F = (1.16639 \pm 0.00002) \times 10^{-5}$ GeV^{-2} [18] is the Fermi coupling constant, and radiative corrections are ignored. This results in

$$f_K = (111.5 \pm 2.3 \pm 0.9) \text{ MeV} \ , \quad (6)$$

where the first error is from the uncertainty on $B(\tau^- \to K^-\nu_\tau)$ and the second from V_{us}.

3 Study of resonance structure and dynamics

The decay dynamics of τ decays involving kaons are investigated via the invariant mass spectra. Due to the small statistics, decay modes other than $(\overline{K}\pi)^-$, $(\overline{K}\pi\pi)^-$ and $(K\overline{K}\pi)^-$ are not discussed here. Even for these, only a qualitative approach based on simple descriptions can be considered.

3.1 Mass spectrum for $\tau^- \to (\overline{K}\pi)^-\nu_\tau$

Three measured modes, $K^-\pi^0$, $K_S^0\pi^-$ and $K_L^0\pi^-$, are used to study the invariant mass of the $\overline{K}\pi$ system. The $K^*(892)^-$ dominance is well established in all the cases [6,7]. For the first two modes, where the mass resolution is good enough, some excess is observed at large mass over and above the expected $K^*(892)^-$ tail. This could arise from a possible $K^*(1410)$ vector state contribution, expected to be dominated by $K^*(892) - K^*(1410)$ interference as already observed for $\rho(770) - \rho(1450)$ in the $\pi^-\pi^0$ system [1]. Theoretically, the decay rate for $\tau^- \to (\overline{K}\pi)^-\nu_\tau$ relative to the electronic width is expressed as [19,20]

$$\begin{aligned} \Gamma_{K\pi}/\Gamma_e \sim \int \frac{ds}{M_\tau^2}\left(1 - \frac{s}{M_\tau^2}\right)^2\left(1 + 2\frac{s}{M_\tau^2}\right) \\ \times \left(s - M_+^2\right)^{3/2}\left(s - M_-^2\right)^{3/2} s^{-3}|f(s)|^2 \ , \end{aligned} \quad (7)$$

where $M_\pm = M_K \pm M_\pi$ and the form factor includes both $K^*(892)$ and $K^*(1410)$ contributions, namely

$$f(s) = \frac{1}{1+\beta}[BW_{K^*(892)}(s) + \beta BW_{K^*(1410)}(s)] \ , \quad (8)$$

[2] The decay constant f_P should be scaled by a factor of $\sqrt{2}$ to compare with the value given in [18]

Table 2. Fit results for $\tau^- \to K^-\pi^0\nu_\tau$ and $\tau^- \to K^0_S\pi^-\nu_\tau$ decays. The errors given are statistical only. Because the background of $\tau^- \to K^-K^0\nu_\tau$ dominates over the higher $K^0_S\pi^-$ invariant mass tail, the background subtraction relies on the model prediction [20] and introduces additional systematic uncertainties in the $K^0_S\pi^-$ system. The fixed values for the masses and widths of the K^* resonances are taken from [18]

Parameter	Fit 1 ($K^-\pi^0$)	Fit 2 ($K^-\pi^0$)	Fit 3 ($K^-\pi^0 + K^0_S\pi^-$)
$M_{K^*(892)}$ (GeV/c^2)	0.895 ± 0.002	0.892	0.892
$\Gamma_{K^*(892)}$ (GeV/c^2)	0.055 ± 0.008	0.050	0.050
β	-0.06 ± 0.07	-0.11 ± 0.05	-0.12 ± 0.04
$M_{K^*(1410)}$ (GeV/c^2)	1.412	1.412	1.412
$\Gamma_{K^*(1410)}$ (GeV/c^2)	0.227	0.227	0.227
χ^2/ndf	13.0/19	16.0/21	19.8/21

where β is assumed to be real [20]. The two Breit-Wigner propagators have the form

$$BW(s) = \frac{M_0^2}{M_0^2 - s - i\sqrt{s}\Gamma(s)} \ , \qquad (9)$$

with an energy dependent width $\Gamma(s)$

$$\Gamma(s) = \Gamma_0 \frac{M_0^2}{s} \left(\frac{p(s)}{p(M_0^2)} \right)^{2l+1} \ , \qquad (10)$$

$$p(s) = \frac{1}{2\sqrt{s}} \sqrt{(s - M_+^2)(s - M_-^2)} \ , \qquad (11)$$

where l is the $K - \pi$ angular momentum, *i.e.*, $l = 1$ for p wave.

The $K^*(1410)$ search is performed using only the $K^-\pi^0$ channel as this has the lowest background in the interference region and the best mass resolution. Figure 1 shows the mass spectrum after background subtraction and bin by bin correction for both resolution and acceptance. The fits using the above parametrization are listed in Table 2. If the mass and width of the $K^*(892)$ are left free (Fit 1), the fitted values are found to be consistent with the world average [18]. With the fixed K^* parameters, the final value is obtained (Fit 2) using the $K^-\pi^0$ data, where the systematic uncertainty from the non-$K\pi$ events is negligible. A fit to the combined $K^-\pi^0$ and $K^0_S\pi^-$ invariant mass distributions is also given (Fit 3).

The measurement of $\beta = -0.11 \pm 0.05$ is, as expected from $SU(3)$ flavour symmetry, in agreement with the $\rho(1450)$ contribution ($\beta = -0.094 \pm 0.007$ from the ALEPH measurement of the decay $\tau^- \to \pi^-\pi^0\nu_\tau$ [1]). Low statistics do not allow much more information to be derived from the fit; however, leaving the phase of β as a free parameter yields a value $(180 \pm 55)^\circ$, consistent with the assumption made.

The relative $K^*(892)$ and $K^*(1410)$ "diagonal" contributions to the $\tau^- \to (\overline{K}\pi)^-\nu_\tau$ branching ratio determined from the value of β are found to be $(97.5^{+1.0}_{-1.4})\%$ and $(0.8^{+0.7}_{-0.5})\%$, respectively, the interference contributing $(1.7^{+0.7}_{-0.5})\%$ for the remainder. According to [18] the decay fraction of $K^*(1410)$ into $\overline{K}\pi$ is $(6.6 \pm 1.3)\%$, and for this analysis the rest is assumed to decay into $\overline{K}\pi\pi$ final states. After correction for the τ kinematic factor (see (34)), this fraction becomes $(7.2 \pm 1.4)\%$ for $K^*(1410)$ produced in τ decays and leads to

$$B(\tau^- \to K^*(1410)^-\nu_\tau) = (1.5^{+1.4}_{-1.0}) \times 10^{-3} \ , \qquad (12)$$

using the $\overline{K}\pi$ branching fraction from Table 1.

In this analysis, a contribution from the scalar $K_0^*(1430)$ has been ignored. No evidence for this state is seen in the $\overline{K}\pi$ mass plot. Nevertheless, a fit with this contribution was performed using the resonance parameters from [18]. A 95% confidence level upper limit of 0.5×10^{-3} is derived for the corresponding branching ratio.

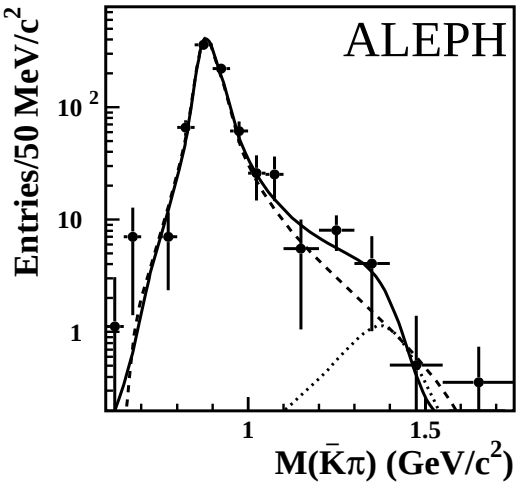

Fig. 1. The invariant mass spectrum for $\tau^- \to K^-\pi^0\nu_\tau$ after background subtraction, bin migration and acceptance corrections. The fit is described by the solid curve, taking into account both $K^*(892)$ and $K^*(1410)$ contributions with interference. The dashed and dotted curves show the $K^*(892)$ and $K^*(1410)$ parts

3.2 Mass spectra for $\tau^- \to (\overline{K}\pi\pi)^-\nu_\tau$

The $(\overline{K}\pi\pi)^-$ decay occurs in the four final states $K^-\pi^+\pi^-$, $K^0_S\pi^-\pi^0$, $K^0_L\pi^-\pi^0$ and $K^-\pi^0\pi^0$. Its invariant mass spec-

trum as well as the spectra for the $\overline{K}\pi$ and $\pi\pi$ subsystems reveal details of the underlying decay dynamics.

3.2.1 Contribution from $K^*(1410)$

The fitted contribution of $K^*(1410)$ found in the previous section has consequences for the $(\overline{K}\pi\pi)^-$ final state, for which the corresponding branching fraction is $(5.97 \pm 0.74) \times 10^{-3}$ as computed from Table 1. The fraction $(92.8 \pm 1.4)\%$ of $K^*(1410)$ decaying into $\overline{K}\pi\pi$ is used to estimate the vector $\overline{K}\pi\pi$ component, while the remainder is attributed to the axial-vector contribution dominated by $K_1(1270)$ and $K_1(1400)$. For the vector current part, one obtains

$$B(\tau^- \to K^*(1410)^-\nu_\tau \to (\overline{K}\pi\pi)^-\nu_\tau) = (1.4\,^{+1.3}_{-0.9}\ ^{+0.0}_{-0.4}) \times 10^{-3}\ , \quad (13)$$

where the first uncertainty comes from the fit to the $\overline{K}\pi$ invariant mass, while the second uncertainty arises from the possibility for the $K^*(1410)$ to decay into $K\eta$. After subtracting this vector component, the axial-vector contribution to the $\overline{K}\pi\pi$ decay modes is

$$B_A(\tau^- \to (\overline{K}\pi\pi)^-\nu_\tau) = (4.6\,^{+1.2}_{-1.5}) \times 10^{-3}\ . \quad (14)$$

3.2.2 $\overline{K}\rho$ and $\overline{K}^*\pi$ fractions

The $\overline{K}\pi$ and $\pi\pi$ mass spectra are used to search for the intermediate states $\overline{K}^*\pi$ and $\overline{K}\rho$. The $\overline{K}\rho$ fraction can reveal the presence of the axial vector $K_1(1270)$ resonance which decays about 50% of the time to $K\rho$ [18], unlike the $K_1(1400)$ which decays almost purely to $\overline{K}^*\pi$. For practical reasons related to the shape of the different backgrounds, the most efficient way for separating the $\overline{K}^*\pi$ and $\overline{K}\rho$ intermediate states is to fit the $\pi\pi$ invariant mass spectra where background and non-$\overline{K}\rho$ contributions are essentially located at lower masses.

No excess in the ρ mass region is found in the $K^-\pi^0\pi^0$ mode, as expected, while a ρ signal is observed in the $K^-\pi^+\pi^-$ mode [5] and also in both the $K^0_S\pi^-\pi^0$ [6] and $K^0_L\pi^-\pi^0$ modes [7]. With the assumption that the $\overline{K}\pi\pi$ final states proceed only via an incoherent superposition of the intermediate states $\overline{K}\rho$ and $\overline{K}^*\pi$, a sum of a ρ Breit-Wigner signal with the τ kinematic factor and the shape of the $\overline{K}^*\pi$ reflections obtained from simulation is used to fit the $\pi\pi$ mass spectrum after subtracting the non-$\overline{K}\pi\pi$ background. It yields the fractions $f_{K^-\rho^0} = (39 \pm 14)\%$ for the $K^-\pi^+\pi^-$ mode[3] and $f_{\overline{K^0}\rho^-} = (74 \pm 13)\%$ for the $\overline{K^0}\pi^-\pi^0$ mode. The sum of the fits to the $\pi\pi$ invariant mass spectra is shown in Fig. 2. These results indicate that the $(\overline{K}\rho)^-$ intermediate state plays an important role in the $\overline{K}\pi\pi$ mode. The smaller value in the $K^-\pi^+\pi^-$ mode is understood from isospin considerations as discussed in Sect. 5. The sum of decays involved in the $\overline{K}\rho$ intermediate state gives $B(\tau^- \to (\overline{K}\rho)^-\nu_\tau) = (3.25 \pm 0.67) \times 10^{-3}$.

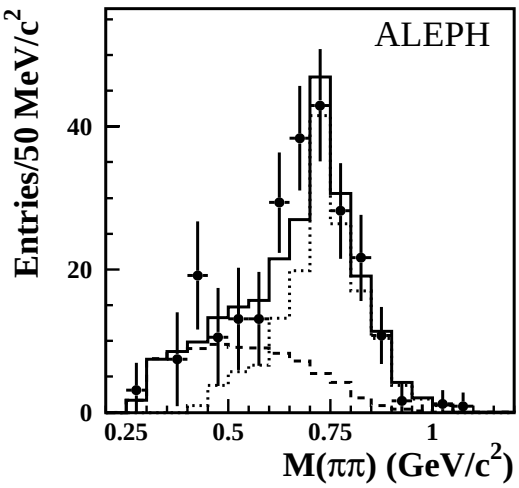

Fig. 2. The $\pi\pi$ invariant mass spectrum for $\tau^- \to (\overline{K}\pi\pi)^-\nu_\tau$ after background subtraction. The overall fit, the expected ρ signal and $\overline{K}^*\pi$ reflection are shown in solid, dotted and dashed histograms

The branching fraction of the $K_1(1270)$ into $K\rho$ is taken from [18] and becomes $(52 \pm 7)\%$, when taking into account the τ kinematic factor. A first estimate of the branching ratio to the $K_1(1270)$ is therefore derived to be

$$B(\tau^- \to K_1^-(1270)\nu_\tau) = (6.3 \pm 1.5) \times 10^{-3}\ \ (\overline{K}\rho \text{ fractions})\ , \quad (15)$$

where all the $\overline{K}\rho$ states are assumed to originate from $K_1(1270)$ decay only.

3.2.3 Fit to $\overline{K}\pi\pi$ resonances

The description of the $\overline{K}\pi\pi$ mass spectrum in terms of the resonant states $K_1(1270)$, $K_1(1400)$ and $K^*(1410)$ is rather complicated because several intermediate states are involved, as discussed in [21,22]. Therefore, the shape of the respective mass distributions is obtained from the Monte Carlo simulation, taking into account all the known intermediate states. The resonance parameters for the $K_1(1270)$, $K_1(1400)$ and $K^*(1410)$ are fixed at 1.273 GeV/c^2, 1.402 GeV/c^2 and 1.412 GeV/c^2 for the masses and at 0.15 GeV/c^2, 0.174 GeVc^2 and 0.227 GeV/c^2 for the widths. The chosen width for the $K_1(1270)$ is different from the value in [18], because of the parametrization adopted: it should be interpreted as an effective width, resulting from the opening of the different decay channels. It has been checked that the resulting line shape agrees well with the existing data [21,22]. However as the value for the width can have a strong effect on the relative fractions in the $K_1(1270)$ decay, an uncertainty of ± 0.05 GeV/c^2 is assigned to it. The mass resolution and the statistics are not sufficient to separate the $K_1(1400)$ and $K^*(1410)$ states,

[3] This value differs slightly from the published result (35±11) in [5] which was obtained with a ρ lineshape inadvertently not corrected for the τ kinematic factor

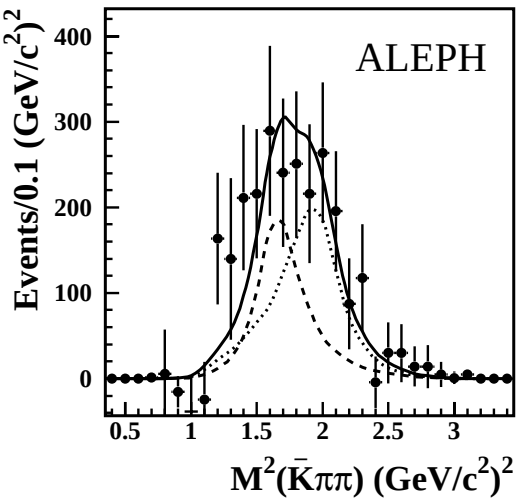

Fig. 3. The invariant mass-squared distribution for $\tau^- \to (\overline{K}\pi\pi)^-\nu_\tau$ after efficiency corrections for the different final states and background subtraction. Data are shown by the dots with error bars. The fit is described by the solid curve, while the expected $K_1(1270)$ and $K_1(1400)$ contributions are separately depicted by the dashed and the dotted curves

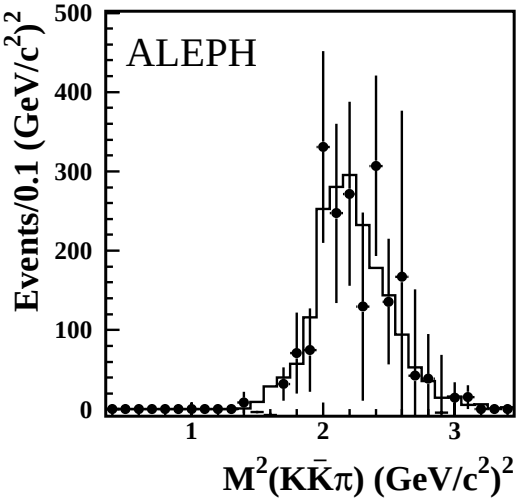

Fig. 4. The invariant mass-squared distribution for $\tau^- \to (K\overline{K}\pi)^-\nu_\tau$ after efficiency corrections for the different final states and background subtraction. Data are shown by the dots with error bars. The histogram represents the model expectation [23]

and so an effective resonance is used instead, averaging the parameters of the two states. To obtain the shapes including all the intermediate states, the $K_1(1270)$ decays into $K\rho$, $K^*(892)\pi$, $K^*(1430)\pi$ and $Kf_0(1370)$ are generated separately and then combined according to the relative fractions given in [18]. Since the τ kinematic factor modifies the branching ratios, the fractions for the different final states are recomputed for $K_1(1270)$ production in τ decays, yielding $(52\pm7)\%$, $(25\pm8)\%$, $(8\pm1)\%$, $(14\pm3)\%$ and $(1\pm1)\%$ for the $K\rho$, $K^*(892)\pi$, $K^*(1430)\pi$ $K\omega$ and Kf_0 final states, respectively. The fit is shown in Fig. 3, giving $\chi^2/ndf = 14.1/22$ and a fraction

$$f_{K_1(1270)} = (41 \pm 19 \pm 15)\% \ , \qquad (16)$$

where the first error is of statistical origin and the second comes from the $K_1(1270)$ width. Because the total branching ratio for the $\overline{K}\pi\pi$ modes is $B(\tau^- \to (\overline{K}\pi\pi)^-\nu_\tau) = (5.97 \pm 0.74) \times 10^{-3}$, the expected branching ratio for $K_1(1270)$ is

$$B(\tau^- \to K_1^-(1270)\nu_\tau) = (2.9 \pm 1.7) \times 10^{-3} \ \ (\overline{K}\pi\pi \text{ fit}) \ , \qquad (17)$$

taking into account the fact that $(86 \pm 3)\%$ of the $K_1(1270)$'s decay into $K\pi\pi$ final states.

The values (15) and (17) obtained from two independent estimates are in fair agreement and their combination yields

$$B(\tau^- \to K_1^-(1270)\nu_\tau) = (4.8 \pm 1.1) \times 10^{-3} \ \ \text{(combined)} \ . \qquad (18)$$

From this value, the τ decay into $K^-\omega$ through $K_1^-(1270)$ is estimated (using the branching ratio in [18]) to be $(0.67 \pm 0.21) \times 10^{-3}$, indicating an axial-vector contribution of $B_A(\tau^- \to K^-\pi^+\pi^-\pi^0\nu_\tau) = (0.59 \pm 0.19) \times 10^{-3}$ in the measured $\overline{K}\pi\pi\pi$ decay modes. Comparing the results in (14) and (18), and using the effective branching fractions of $(86 \pm 3)\%$ and 100% [18] for the decay of $K_1^-(1270)$ and $K_1^-(1400)$ into $K\pi\pi$, one obtains a branching ratio $B(\tau^- \to K_1^-(1400)\nu_\tau) = (0.5\pm1.7)\times10^{-3}$, which is somewhat reduced in comparison with that of $K_1^-(1270)$.

3.3 Mass spectra for $\tau^- \to (K\overline{K}\pi)^-\nu_\tau$

Almost all possible final states for $(K\overline{K}\pi)^-$ are studied by ALEPH (Table 1): $K^+K^-\pi^-$, $K^0_SK^0_S\pi^-$, $K^0_SK^0_L\pi^-$, $K^-K^0_S\pi^0$ and $K^-K^0_L\pi^0$. The $K^+\pi^-$ mass plot in the $K^+K^-\pi^-$ mode shows a clear $K^*(892)^0$ signal, and a fit yields a fraction of $(87 \pm 13)\%$ for the K^*K^- component [5]. A strong $K^*(892)^-$ signal is also found in the $K^-K^0_L\pi^0$ mode with an estimated lower limit of 86% at 90% confidence level for the $\overline{K}^*(K^*)$ component [7], confirming the conclusion of K^* dominance in the $K\overline{K}\pi$ mode.

Both the $K^+K^-\pi^-$ and $K^-K^0_S\pi^0$ modes are used to measure the total $K\overline{K}\pi$ invariant mass distribution, scaling their rates by a factor of two. Figure 4 shows the combined $K\overline{K}\pi$ invariant mass-squared distribution after correcting for resolution and efficiency. The Monte Carlo expectation [23], based on a_1 dominance, is observed to be consistent with the data.

4 Tests of isospin invariance

Isospin relations relevant to τ decays into kaons have been established in [24–26]. The set of results obtained by ALEPH allows for a complete test of these relations. Apart from testing isospin invariance in the hadronic states accessible in τ decays, this procedure can be helpful as a consistency check among the different final states, regardless of the decay dynamics.

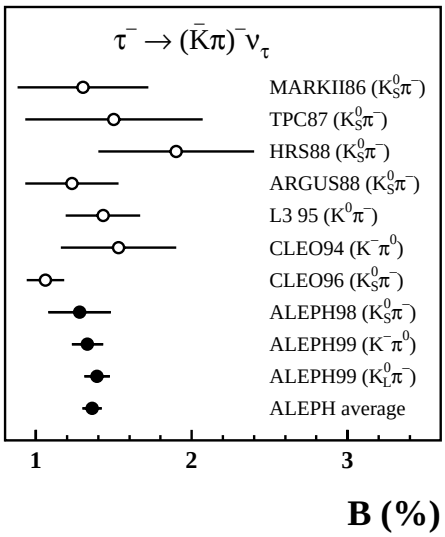

Fig. 5. The published branching ratios for $\tau^- \to (\overline{K}\pi)^-\nu_\tau$ [6, 7,27], using all three measured modes and assuming $I = 1/2$

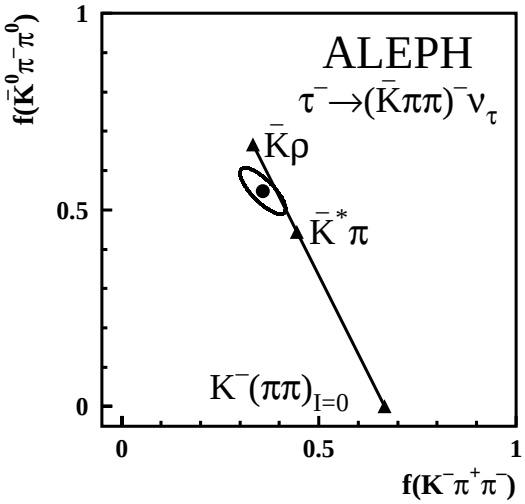

Fig. 6. The decay fractions for $K^-\pi^+\pi^-\nu_\tau$ and $\overline{K^0}\pi^0\pi^-\nu_\tau$ given by the standard error ellipse (39% probability). The isospin constraint is shown by the straight line. The triangles indicate possible intermediate states dominated by $\overline{K}^*\pi$, $\overline{K}\rho$ or $K^-(\pi\pi)_{I=0}$

4.1 The decay $\tau^- \to (\overline{K}\pi)^-\nu_\tau$

The branching ratios of the three final states of the decay $\tau^- \to (\overline{K}\pi)^-\nu_\tau$, respectively, $K^-\pi^0$, $K^0_S\pi^-$ and $K^0_L\pi^-$, are presented in Table 1. A study of the corresponding invariant mass spectra shows that the decay is dominated by $K^*(892)$, with a small component of $K^*(1410)$ visible through its interference with $K^*(892)$ as presented in Sect. 3.1. Isospin symmetry for an $I = 1/2$ state, together with the assumption of equal K^0_S and K^0_L contributions, constraints the rates for the three final states to be equal up to small mass corrections. Taking this into account, the above three measurements are well consistent with isospin symmetry, giving a $\chi^2/ndf = 0.9/2$. Using isospin symmetry as a constraint yields the total branching ratio

$$B(\tau^- \to (\overline{K}\pi)^-\nu_\tau) = (13.60 \pm 0.62) \times 10^{-3} \ . \qquad (19)$$

A comparison between this analysis and the other measurements is shown in Fig. 5.

From the fit performed in Sect. 3.1, the branching ratio for $K^*(892)^-$ production is found to be

$$B(\tau^- \to K^*(892)^-\nu_\tau) = (13.26 \pm 0.63) \times 10^{-3} \ . \qquad (20)$$

4.2 The decay $\tau^- \to (\overline{K}\pi\pi)^-\nu_\tau$

For a total isospin $I = 1/2$ and the two possible isospin values $I_{\pi\pi} = 0, 1$ for the $\pi\pi$ system, a relation can be established among the branching ratios of the $\overline{K^0}\pi^-\pi^0$, $K^-\pi^+\pi^-$ and $K^-\pi^0\pi^0$ modes [25]:

$$B(\tau^- \to K^-\pi^+\pi^-\nu_\tau) \qquad (21)$$
$$= \frac{1}{2}B(\tau^- \to \overline{K^0}\pi^-\pi^0\nu_\tau) + 2B(\tau^- \to K^-\pi^0\pi^0\nu_\tau) \ .$$

In order to examine to what extent the above isospin constraint is satisfied by experiment, it is convenient to use the relative fractions of the total $\overline{K}\pi\pi$ branching ratio for each individual mode. This gives $f(\overline{K^0}\pi^-\pi^0) = 0.55 \pm 0.06$, $f(K^-\pi^+\pi^-) = 0.36 \pm 0.06$, and $f(K^-\pi^0\pi^0) = 0.09 \pm 0.04$ from the ALEPH measurements with a correlation coefficient of -0.8 between $f(\overline{K^0}\pi^-\pi^0)$ and $f(K^-\pi^+\pi^-)$. The corresponding error ellipse is given in Fig. 6, showing that the isospin relation (21) is satisfied within one standard deviation.

Table 3. The relative fraction for each $\overline{K}\pi\pi$ mode from isospin symmetry for the possible intermediate states. The test of these fractions is given by the χ^2/ndf values for the hypothesis that the given intermediate state dominates

Mode	$K^-\pi^+\pi^-$	$\overline{K^0}\pi^-\pi^0$	$K^-\pi^0\pi^0$	χ^2/ndf
$\overline{K}\rho$	1/3	2/3	0	7.0/3
$\overline{K}^*\pi$	4/9	4/9	1/9	2.8/3
$K^-(\pi\pi)_{I=0}$	2/3	0	1/3	88.7/3

The isospin relations can be tested in more detail if the different intermediate states are separated. Three possible intermediate states occurring in the $(\overline{K}\pi\pi)^-$ final state are considered: $\overline{K}\rho$ and $K^-(\pi\pi)_{I=0}$ corresponding to $I_{\pi\pi} = 1$ and 0, respectively, and $\overline{K}^*\pi$, with the expected relative rates in the different final states as given in Table 3. It turns out that a pure $K^-(\pi\pi)_{I=0}$ is excluded by the measurement, while a combination of $\overline{K}\rho$ and $\overline{K}^*\pi$ can fit the data well. This is in agreement with the findings of the resonance structure analysis performed in Sect. 3.2.2. A further check of the isospin symmetry is achieved taking advantage of the $\overline{K}\rho$ and $\overline{K}^*\pi$ separation provided by the ρ resonance fits performed in the two relevant channels. The results given in Table 4 are in agreement with the expectations.

Table 4. Test of isospin symmetry for different intermediate states. The separation of the branching ratios for $\overline{K}\rho$ and $\overline{K}^*\pi$ is based on the measurements of the $\overline{K}\rho$ fractions. The χ^2/ndf values represent the consistency with the expected relative ratios given in Table 3

Mode	$K^-\pi^+\pi^-$ (10^{-3})	$\overline{K^0}\pi^-\pi^0$ (10^{-3})	$K^-\pi^0\pi^0$ (10^{-3})	χ^2/ndf
$\overline{K}\rho$	0.83 ± 0.35	2.42 ± 0.57	0	0.7/3
$\overline{K}^*\pi$	1.31 ± 0.41	0.85 ± 0.45	0.56 ± 0.25	1.8/3

Table 5. The relative fractions for each $\overline{K}\pi\pi\pi$ mode expected by isospin invariance for $I_{3\pi} = 1$. The three numbers $(n_1 n_2 n_3)$ label Pais' isospin classes [28]. The test of isospin symmetry is given by the χ^2/ndf values for the hypothesis that the given intermediate state dominates

Class	$K^-\pi^+\pi^-\pi^0$	$K^-\pi^0\pi^0\pi^0$	$\overline{K^0}\pi^+\pi^-\pi^-$	$\overline{K^0}\pi^-\pi^0\pi^0$	$B(\overline{K}3\pi)$ (10^{-3})	χ^2/ndf
(300)	2/15	1/5	8/15	2/15	0.65 ± 0.39	1.8/3
(210)	1/3	0	1/3	1/3	0.83 ± 0.46	3.0/3

4.3 The decay $\tau^- \to (\overline{K}\pi\pi\pi)^-\nu_\tau$

The final states considered include $K^-\pi^+\pi^-\pi^0$, $K^-\pi^0\pi^0$ π^0, $K^0h^+h^-h^-$ and $\overline{K^0}\pi^-\pi^0\pi^0$, in which the $K^-\eta$ contributions are excluded. Since the net strangeness for the $K^0h^+h^-h^-$ modes is not determined, $\overline{K^0}\pi^+\pi^-\pi^-$ dominance is assumed. Isospin invariance for the 3π system leads to only three symmetry classes [25,28]: two with $I_{3\pi} = 1$, as shown in Table 5, and one with $I_{3\pi} = 0$, expected to be dominated by the $K^-\omega$ state. An axial-vector contribution from the decay $K_1^-(1270) \to K^-\omega \to K^-\pi^+\pi^-\pi^0$, amounting to $(0.59 \pm 0.19) \times 10^{-3}$, was deduced in Sect. 4.2 and is subtracted from the $K^-\pi^+\pi^-\pi^0$ mode.

The expected relative contributions from the $I_{3\pi} = 1$ classes are compared to data in Table 5. The present experimental precision does not allow definite conclusions. However, the different isospin configurations can be used to derive a better estimate of the total rate. The two isospin possibilities lead to consistent values (see Table 5) and the average using the Fermi statistical weights [28] yields (excluding the $K^-\omega$ mode)

$$B(\tau^- \to (\overline{K}\pi\pi\pi)^-\nu_\tau) = (0.76 \pm 0.44) \times 10^{-3} \ . \qquad (22)$$

4.4 The decay $\tau^- \to (K\overline{K}\pi)^-\nu_\tau$

For this mode, the decay dynamics are investigated using the branching ratios for all the relevant final states: $K^+K^-\pi^-$, $K_S^0K^-\pi^0$, $K_L^0K^-\pi^0$, $K_S^0K_L^0\pi^-$ and $K_S^0K_S^0\pi^-$, as shown in Table 1. If the contribution of second-class currents is ignored, the rates for $K^+K^-\pi^-$ and $K^0\overline{K^0}\pi^-$ are expected to be equal [25], in agreement with the measurement

$$\frac{B(\tau^- \to K^0\overline{K^0}\pi^-\nu_\tau)}{B(\tau^- \to K^+K^-\pi^-\nu_\tau)} = 0.94 \pm 0.27 \ . \qquad (23)$$

The possible intermediate states appearing in these decay modes are considered to be $\overline{K^*}K + K^*\overline{K}$ (denoted K^*K), $\rho\pi$ and $\pi(K\overline{K})_{I=0}$, corresponding to the fractions shown in Table 6. The test of isospin symmetry is consistent with the K^*K intermediate state as illustrated in Fig. 7, in agreement with the conclusion from the analysis of the $K\pi$ mass spectra.

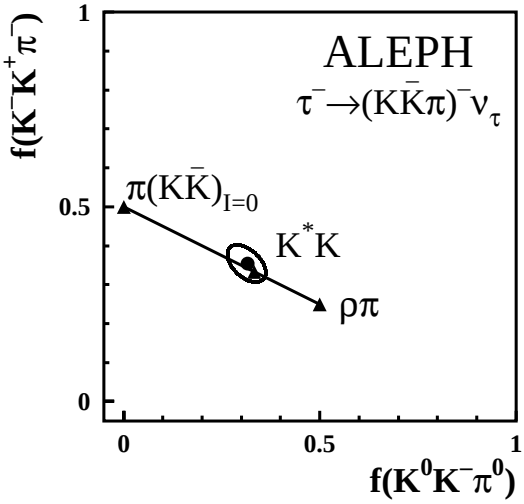

Fig. 7. The decay fractions for $K^0K^-\pi^0\nu_\tau$ and $K^-K^+\pi^-\nu_\tau$, given by a standard ellipse (39% probability), are compared to the isospin constraint on the $K\overline{K}\pi$ mode, shown by the straight line. The triangles indicate the intermediate states dominated by $\pi(K\overline{K})_{I=0}$, K^*K or $\rho\pi$

4.5 The decay $\tau^- \to (K\overline{K}\pi\pi)^-\nu_\tau$

The limited experimental information (see Table 1) on $K\overline{K}\pi\pi$ final states makes it impossible to study this channel in any detail. Nevertheless, some conclusions can still be drawn. First, the rates for $\tau^- \to K^+K^-\pi^-\pi^0\nu_\tau$ and $\tau^- \to K^0\overline{K^0}\pi^-\pi^0\nu_\tau$ are consistent within their uncertainties, as expected by isospin symmetry and the absence of second-class currents [25]. Then, the relative fractions observed in the different modes can be compared with the

Table 6. The relative fraction for each $K\overline{K}\pi$ mode in view of isospin relations for three possible intermediate states. The test of these relations is given by the χ^2/ndf values for the hypothesis that the given intermediate state dominates

Mode	$K^-K^+\pi^-$	$K^0_SK^0_L\pi^-$	$K^0_SK^0_S\pi^- + K^0_LK^0_L\pi^-$	$K^-K^0\pi^0$	χ^2/ndf
K^*K	1/3	1/6	1/6	1/3	2.1/3
$\rho\pi$	1/4	1/4	0	1/2	16.0/3
$\pi(K\overline{K})_{I=0}$	1/2	0	1/2	0	99.0/3

expectations from the possible isospin configurations [26], with a strong preference for the ($I_{K\overline{K}} = 0,\ I_{\pi\pi} = 1$) states and to a lesser extent ($I_{K\overline{K}} = 1,\ I_{\pi\pi} = 1$). The weighted average over the two non-zero modes yields an estimate for the total rate

$$B(\tau^- \to (K\overline{K}\pi\pi)^-\nu_\tau) = (0.5 \pm 0.2) \times 10^{-3}\ . \qquad (24)$$

5 Vector and axial-vector separation

The separation of the τ final states into vector and axial-vector currents provides important information for QCD studies. Any deviation between the inclusive sums of vector and axial-vector hadronic branching ratios is necessarily a result of nonperturbative phenomena. In this section, all the information obtained on the strange decay fractions concerning their V/A character are summarized in order to determine the corresponding inclusive rates. In addition, the separation of vector and axial-vector components is presented for the nonstrange $K\overline{K}\pi$ mode.

5.1 $\tau^- \to (\overline{K}n\pi)^-\nu_\tau$

The branching ratios for the strange sector of τ decays are globally reconsidered in Table 7, with the respective current contributions unambiguously separated for the K^-, $(\overline{K}\pi)^-$, $K^-\eta$ and $(\overline{K}\pi\pi)^-$ modes. In the $(\overline{K}3\pi)^-$ mode, the contribution expected from the axial-vector $K_1(1270)$ decay into $K^-\omega$ is subtracted. The total $(\overline{K}4\pi)^-$ and $(\overline{K}5\pi)^-$ contributions are estimated on the basis of the branching ratios for the 5π and 6π modes [18] with Cabibbo and kinematic suppression, even though the resulting total contribution is small in comparison to the precision achieved in the measurement of the strange sector of τ decays. For the non-$K^-\omega$ part of $(\overline{K}3\pi)^-$, the $(\overline{K}4\pi)^-$ and the $(\overline{K}5\pi)^-$ contributions, it is assumed that vector and axial-vector contribute equally with 100% anti-correlated errors. The corresponding branching ratios for vector and axial-vector final states are

$$B(\tau^- \to V^-(S=-1)\nu_\tau) = (15.9\ ^{+1.6}_{-1.4}) \times 10^{-3} \qquad (25)$$

and

$$B(\tau^- \to A^-(S=-1)\nu_\tau) = (12.8\ ^{+1.4}_{-1.7}) \times 10^{-3}\ . \qquad (26)$$

The total branching ratio for all strange τ decays

$$B(\tau^- \to (V+A)^-(S=-1)\nu_\tau) = (28.7 \pm 1.2) \times 10^{-3} \qquad (27)$$

Table 7. Branching ratios for vector and axial vector current contributions to the strange sector of τ decays. The branching fractions for the $\overline{K}4\pi$ and $\overline{K}5\pi$ modes are obtained from the measured branching ratios for the 5π and 6π in [18] introducing the Cabibbo suppression and kinematic factors. Vector and axial vector currents in the $\overline{K}3\pi$, $\overline{K}4\pi$ and $\overline{K}5\pi$ are assumed to contribute equally

Mode	B_V (10^{-3})	B_A (10^{-3})	B_{V+A} (10^{-3})
K^-	–	6.96 ± 0.29	6.96 ± 0.29
$(\overline{K}\pi)^-$	13.60 ± 0.62	–	13.60 ± 0.62
$(\overline{K}2\pi)^-$	$1.39\ ^{+1.30}_{-1.01}$	$4.58\ ^{+1.23}_{-1.49}$	5.97 ± 0.74
$K_1^-(1270) \to K^-\omega$	–	0.67 ± 0.21	0.67 ± 0.21
$K^-\eta$	$0.29\ ^{+0.15}_{-0.14}$	–	$0.29\ ^{+0.15}_{-0.14}$
$(\overline{K}3\pi)^-$	0.38 ± 0.53	0.38 ± 0.53	0.76 ± 0.44
$(\overline{K}4\pi)^-$	0.17 ± 0.37	0.17 ± 0.37	0.34 ± 0.34
$(\overline{K}5\pi)^-$	0.03 ± 0.10	0.03 ± 0.10	0.06 ± 0.06
Sum	$15.86\ ^{+1.60}_{-1.37}$	$12.79\ ^{+1.43}_{-1.66}$	28.65 ± 1.17

is known with better precision.

An estimate of the size of nonperturbative QCD contributions can be obtained from the ratio

$$\frac{B(\tau^- \to V^-(S=-1)\nu_\tau) - B(\tau^- \to A^-(S=-1)\nu_\tau)}{B(\tau^- \to (V+A)^-(S=-1)\nu_\tau)} = (11\ ^{+10}_{-8})\%\ , \qquad (28)$$

which is consistent with zero, but cannot rule out a significant nonperturbative component. In comparison, the value $(1.7 \pm 1.0)\%$ was obtained in the nonstrange sector of τ decays [2].

5.2 $\tau^- \to (K\overline{K}\pi)^-\nu_\tau$

In the analysis of the nonstrange spectral functions [1,2], fractions of $(50 \pm 50)\%$ vector and axial-vector currents were assumed for lack of a better knowledge in $\tau^- \to (K\overline{K}\pi)^-\nu_\tau$ decays. Due to the anti-correlation between vector and axial-vector, this uncertainty was important for the difference $V - A$.

In this analysis, two methods are considered in order to separate the vector and axial-vector contributions in the $K\overline{K}\pi$ mode. The first method based on the G-parity [25] applies best to the cases of either a pure vector or a pure axial-vector state. The second method is to compare the inclusive $V + A$ $K\overline{K}\pi$ spectral function of τ decays with

the corresponding isovector cross section measurements in e^+e^- annihilation, providing the V part by means of CVC.

The G-parity of the $K\overline{K}\pi$ system is determined by the $K\overline{K}$ system with $G_{K\overline{K}} = (-1)^{I_{K\overline{K}}}(-1)^{l_{K\overline{K}}}$. Since the $K^0K^-\pi^0$ mode can only have $I_{K\overline{K}} = 1$, the corresponding decay width amounts to half of the total decay width for $I_{K\overline{K}} = 1$. The isospin configuration $I_{K\overline{K}} = 0$ contributes to both the $K^0\overline{K^0}\pi^-$ and $K^+K^-\pi^-$ modes. In addition, the $l_{K\overline{K}}$ values are always odd for $K^0_SK^0_L$ and even for $K^0_SK^0_S$ or $K^0_LK^0_L$. The two following ratios are therefore defined [25]:

$$r_0 = \frac{\Gamma_{K^0_SK^0_S\pi^-} + \Gamma_{K^0_LK^0_L\pi^-}}{\Gamma_{K^0_SK^0_L\pi^-}} = \frac{2\Gamma^0_A + \Gamma^1_V}{2\Gamma^0_V + \Gamma^1_A} \ , \qquad (29)$$

and

$$r = \frac{\Gamma_{K^0\overline{K^0}\pi^-} + \Gamma_{K^+K^-\pi^-} - \Gamma_{K^0K^-\pi^0}}{\Gamma_{K^0K^-\pi^0}} = 2\frac{\Gamma^0_A + \Gamma^0_V}{\Gamma^1_A + \Gamma^1_V} \ , \qquad (30)$$

where $\Gamma^0_{V,A}$ and $\Gamma^1_{V,A}$ are the decay widths for the $I_{K\overline{K}} = 0$ and $I_{K\overline{K}} = 1$ states, respectively. For pure vector, one has $1/r = r_0$, whereas $r = r_0$ for pure axial vector. The branching ratio measurements from ALEPH give

$$r_0 = 0.52^{+0.32}_{-0.25} \qquad (31)$$

and

$$r = 1.19^{+0.60}_{-0.45} \ . \qquad (32)$$

Consequently, the probabilities for the $K\overline{K}\pi$ mode being a pure axial vector and a pure vector are computed to be about 25% and 50%, respectively. It is therefore not possible to draw a firm conclusion from this study. This is not too surprising as the $K\overline{K}\pi$ mode is observed to be dominated by K^*K, in which case the previous test becomes degenerate.

Another possibility is the comparison between the measured spectral function in τ decay and the measured isovector cross sections in $e^+e^- \to K\overline{K}\pi$. The application of CVC makes it possible to link the τ decays into $K\overline{K}\pi$ final states with e^+e^- annihilation into isovector states $K^0_SK^\pm\pi^\mp$ and $K^\pm K^\mp\pi^0$, via the relation

$$\sigma^{I=1}_{e^+e^-\to K\overline{K}\pi} = \frac{4\pi\alpha^2}{s} v_{1,K\overline{K}\pi\nu_\tau} \ , \qquad (33)$$

where $\sigma^{I=1}_{e^+e^-\to K\overline{K}\pi}$ is the isovector cross section, α is the electromagnetic fine structure constant, and $v_{1,K\overline{K}\pi\nu_\tau}$ is the corresponding vector τ spectral function. There is only isovector in τ decay, while the isospin for the $K\overline{K}\pi$ system in e^+e^- annihilation can be either 0 or 1. By studying the Dalitz plot, the DM1 [29] and DM2 [30] experiments observed K^*K dominance and concluded that the reaction $e^+e^- \to K\overline{K}\pi$ is dominated by the isoscalar (resonant) amplitude, whereas a small isovector component is extracted from the interference of both amplitudes.

The measured invariant mass-squared distribution of the $K\overline{K}\pi$ system in τ decay (Fig. 4) is transformed into the $V + A$ spectral function (according to (34) in the next section). The cross section measurements for $e^+e^- \to K\overline{K}\pi$ [29,30] are also converted into a spectral function according to (33). Since the DM1 and DM2 experiments only provide studies of $K^0_SK^\pm\pi^\mp$, the full $K\overline{K}\pi$ spectrum is obtained by scaling up the $K^0_SK^\pm\pi^\mp$ contribution by a factor of three. Figure 8 shows the comparison between τ decay and e^+e^- annihilation. A fairly large excess is observed below 2.5 $(\mathrm{GeV}/c^2)^2$ compared to the $I = 1$ e^+e^- data. The measured cross sections of $e^+e^- \to K\overline{K}\pi$ are translated by CVC into the expected vector branching ratio $B_V(\tau^- \to (K\overline{K}\pi)^-\nu_\tau)$, yielding $(0.67 \pm 0.27) \times 10^{-3}$ for the DM1 measurement and $-(0.12 \pm 0.26) \times 10^{-3}$ for the DM2 measurement, which are averaged to $(0.26 \pm 0.39) \times 10^{-3}$. This value is much smaller than the measured branching ratio $B(\tau^- \to (K\overline{K}\pi)^-\nu_\tau) = (4.60 \pm 0.50) \times 10^{-3}$, yielding a dominant axial-vector fraction of $(94^{+6}_{-8})\%$.

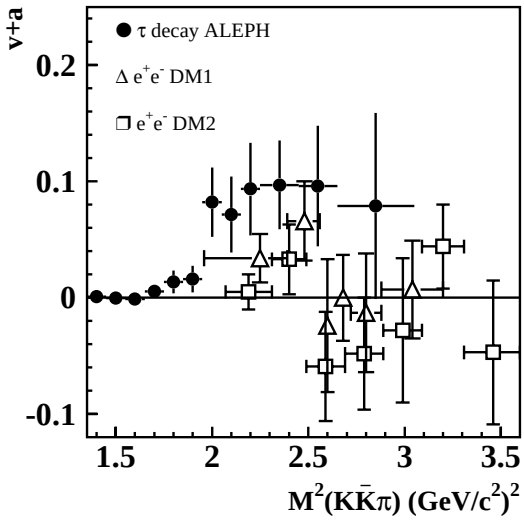

Fig. 8. The $V + A$ spectral function using the $K\overline{K}\pi$ data from τ decays compared to those derived from the isovector e^+e^- cross sections. The e^+e^- data are taken from DM1 [29] and DM2 [30]

One can combine all the information sensitive to the V and A fractions: relative rates of different $K\overline{K}\pi$ modes in τ decay and comparison of total rates in τ decays and $I = 1$ e^+e^- annihilation. It is found that the $I_{K\overline{K}} = 1$ component in the dominant axial-vector part is $(75 \pm 9)\%$, while in the much smaller vector part it amounts to $(43 \pm 28)\%$. These fractions agree with the expected value of 2/3 for K^*K dominance, established for the axial-vector current in this paper, and for the vector current in e^+e^- annihilation [29,30].

A natural candidate to explain the dynamics of the $K\overline{K}\pi$ mode is the decay $a_1 \to K^*K$. In fact the observed mass spectrum agrees well with the Monte Carlo prediction based on this model (Fig. 4), showing a sharp rise at the K^*K threshold. Under the assumption of a_1 dominance and using the branching ratio $B(\tau \to a_1\nu_\tau)$ [31], one gets the branching fraction $B(a_1 \to K^*K) = (2.6 \pm 0.3)\%$. This value is in good agreement with the preliminary re-

sult from a partial wave analysis [32] in the $\tau \to \pi\pi^0\pi^0\nu_\tau$ channel, including the opening of the K^*K decay channel in the a_1 total width, yielding $B(a_1 \to K^*K) = (3.3 \pm 0.5 \pm 0.1)\%$. This observation provides an additional and independent argument for axial-vector dominance in the $K\overline{K}\pi$ mode.

The observed axial-vector dominance is in qualitative agreement with the models developed in [20,23] and in contradiction with those proposed in [33,34].

6 The total strange spectral function

Theoretically, the hadronic τ decay width can be formulated in terms of the spectral functions [35] $v_1(s)$, $a_1(s)$ and $a_0(s)$ for the nonstrange part, and $v_1^S(s)$, $a_1^S(s)$, $v_0^S(s)$ and $a_0^S(s)$ for the strange part, where s is the hadronic mass-squared. The notations v and a stand for vector and axial-vector, while the subscript refers to the spin J of the hadronic system. These spectral functions can be experimentally determined by measuring the invariant mass spectra of given hadronic modes and normalizing them to their respective branching ratios. The nonstrange spectral functions (v_1/a_1 and a_0) are defined and measured in [1, 2], and the strange spectral functions read

$$\begin{aligned} & v_1^S(s)/a_1^S(s) \\ & \equiv \frac{M_\tau^2}{6|V_{us}|^2 S_{EW}} \frac{B(\tau^- \to V^-/A^-(S=-1, J=1)\nu_\tau)}{B(\tau^- \to e^-\bar{\nu}_e\nu_\tau)} \\ & \quad \times \frac{1}{N_{V/A}} \frac{dN_{V/A}}{ds} \left[\left(1 - \frac{s}{M_\tau^2}\right)^2 \left(1 + \frac{2s}{M_\tau^2}\right) \right]^{-1} \end{aligned} \tag{34}$$

and

$$\begin{aligned} & v_0^S(s)/a_0^S(s) \\ & \equiv \frac{M_\tau^2}{6|V_{us}|^2 S_{EW}} \frac{B(\tau^- \to V^-/A^-(S=-1, J=0)\nu_\tau)}{B(\tau^- \to e^-\bar{\nu}_e\nu_\tau)} \\ & \quad \times \frac{1}{N_{V/A}} \frac{dN_{V/A}}{ds} \left(1 - \frac{s}{M_\tau^2}\right)^{-2} , \end{aligned} \tag{35}$$

where $|V_{us}| = 0.2218 \pm 0.0016$ [18], $M_\tau = (1776.9^{+0.31}_{-0.27})$ MeV/c^2 is taken from the BES measurement [36], $S_{EW} = 1.0194 \pm 0.0040$ accounts for the electroweak radiative corrections [37], and $dN_{V/A}/N_{V/A}ds$ denotes the normalized distribution of the invariant mass-squared of the corresponding vector/axial-vector decay channels V/A. The leptonic branching ratio is taken to be $B(\tau^- \to e^-\bar{\nu}_e\nu_\tau) = (17.794 \pm 0.045)\%$, where the precision has been improved by applying lepton universality as described in [2]. The dominant contribution to $a_0^S(s)$ is expected to be provided by the single kaon pole with $a_{0,K}^S(s) = 4\pi^2 f_K^2 \delta(s - M_K^2)$.

Because the spectral functions measure the transition probability to create hadrons with a mass $\sqrt{s}$ from the QCD vacuum, they are the natural input to QCD studies, allowing tests to be performed at a running mass scale less than or equal to M_τ. Their nonstrange vector part can be directly related to the low energy e^+e^- annihilation cross section using CVC. In addition, the strange spectral function carries information on the strange quark mass.

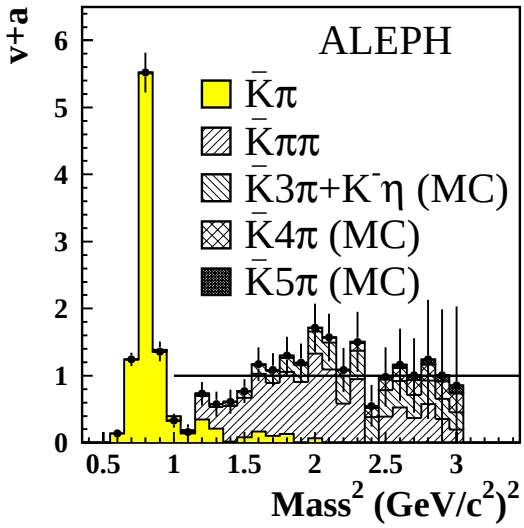

Fig. 9. Measurement of the total hadronic vector and axial-vector spectral function (dots with error bars) from τ decays into strange final states with its different contributions indicated. The errors include systematic uncertainties. The kaon pole is not shown in this plot. The shapes for the $K^-\eta$ and $\overline{K}n\pi(n \geq 3)$ modes are obtained from the Monte Carlo simulation. The parton model prediction is given by the solid straight line

The total strange spectral function is shown in Fig. 9. The spectra for the $\overline{K}\pi$ and $\overline{K}\pi\pi$ modes are obtained from the corrected mass spectra, taking into account the acceptance and bin migration corrections. For the other modes a phase space generator is used to simulate the corresponding mass distributions. The contributions from the respective channels are normalized to the corresponding branching ratios according to (34).

The $K^*(892)^-$ resonance stands out clearly on the low mass side, while within a large uncertainty (dominated by background subtraction in the $(\overline{K}\pi\pi)^-$ modes) the higher energy part is consistent with the parton model expectation.

The total strange spectral function is used in the following section, in order to construct spectral moments needed for the QCD analysis.

7 The strange quark mass

A main goal of the present analysis is the determination of the strange quark mass m_s. The method adopted follows the line of the recent ALEPH $\alpha_s(M_\tau^2)$ determination from nonstrange hadronic τ decays [2] and is based on a simultaneous fit of QCD parametrizations, including perturbative and nonperturbative components, to measured observables. A more detailed account of this method and of the phenomenological context can be found in [15].

7.1 The strange hadronic decay ratio $R_{\tau,S}$

As previously demonstrated in [3], the inclusive τ decay ratio into strange hadronic final states,

$$R_{\tau,S} = \frac{\Gamma(\tau^- \to \text{hadrons}^-_{S=-1}\,\nu_\tau)}{\Gamma(\tau^- \to e^-\,\bar{\nu}_e\nu_\tau)}\ , \tag{36}$$

can be used due to its precise theoretical prediction [10, 11] in the framework of the Operator Product Expansion (OPE) [38] to determine $m_s(s)$ at the scale $s = M_\tau^2$. Since then it was shown [12] that the perturbative expansion used for the massive term in [11] was incorrect. After correction the series shows a problematic convergence behaviour [12–14].

Following [10] the theoretical prediction for the inclusive vector plus axial-vector hadronic decay rate is given by

$$\begin{aligned} &R_\tau(M_\tau^2) \\ &= 12\pi S_{\text{EW}} \int\limits_0^{M_\tau^2} \frac{ds}{M_\tau^2}\left(1-\frac{s}{M_\tau^2}\right)^2 \\ &\times\left[\left(1+2\frac{s}{M_\tau^2}\right)\text{Im}\Pi^{(1+0)}(s)\ -\ 2\frac{s}{M_\tau^2}\text{Im}\Pi^{(0)}(s)\right], \end{aligned} \tag{37}$$

with the two-point correlation functions $\Pi^{(J)} = |V_{ud}|^2\Pi^{(J)}_{ud,V+A} + |V_{us}|^2\Pi^{(J)}_{us,V+A}$ for the hadronic final state of the spin J. The choice of the particular spin combination for the correlators taken in (37) is justified in [10]. Equation (37) can be decomposed as

$$\begin{aligned} R_{\tau,(S)} &= 3|V|^2 S_{\text{EW}} \\ &\times\left(1+\delta^{(0)}+\delta^{(2-\text{mass})}+\sum_{D=4,6,\ldots}\delta^{(D)}+\delta'_{\text{EW}}\right), \end{aligned} \tag{38}$$

where $V = V_{ud}$ ($V = V_{us}$) for the nonstrange (strange) case is the corresponding CKM matrix element. The residual non-logarithmic electroweak correction $\delta'_{\text{EW}} \simeq 0.0010$ [39] is neglected in the following. Throughout this analysis, all QCD observables are expressed in the $\overline{\text{MS}}$ renormalization scheme.

7.1.1 Perturbative contributions

The $\delta^{(0)}$ term in (38) is the perturbative part of mass dimension $D = 0$, known to third order [40] in the expansion with $a_s(M_\tau^2) = \alpha_s(M_\tau^2)/\pi$, and studied in detail in [2].

Next, the $\delta^{(2-\text{mass})}$ term is the mass contribution of dimension $D = 2$, in practice only important for the strange quark mass and the subject of the present study. The fixed-order perturbation theory (FOPT) gives [11,12]

$$\begin{aligned} \delta_S^{(2-\text{mass})} = -8\frac{m_s^2(M_\tau^2)}{M_\tau^2}\Bigg[1+\frac{16}{3}a_s(M_\tau^2)+46.00\,a_s^2(M_\tau^2) \\ +\left(283.6+\frac{3}{4}\,x_3^{(1+0)}\right)a_s^3(M_\tau^2)\Bigg]\ . \end{aligned} \tag{39}$$

The third order coefficient $x_3^{(1+0)}$ occurs in the expansion of the massive $J = 1+0$ correlator [11,41,42], while the $J = 0$ correlator is known up to third order. Assuming the perturbative expansions to behave like a geometric series, one can estimate the unknown coefficient to be $x_3^{(1+0)} \approx x_2^{(1+0)}(x_2^{(1+0)}/x_1^{(1+0)}) = 165 \pm 330$, using as error twice the estimated contribution. Setting $\alpha_s(M_\tau^2) = 0.334$ [2], (39) becomes

$$\begin{aligned} \delta_S^{(2-\text{mass})} &= -8\frac{m_s^2(M_\tau^2)}{M_\tau^2} \\ &\times[1+0.57+0.52+(0.49\pm0.29)]\ , \end{aligned} \tag{40}$$

which converges badly.

A so-called *contour-improved* FOPT [43,44] analysis (FOPT_{CI}) for the dimension $D = 2$ contribution has been presented in [13,14]. It consists of a direct numerical evaluation of the contour integral derived from (37), using the solution of the renormalization group equation (RGE) to four loops [45,46] as input for the running $\alpha_s(s)$ and $m_s(s)$. This provides a resummation of all known higher order logarithmic integrals and was observed to improve the convergence of the massless perturbative series [2,43]. With the above value for α_s, the contour-improved evaluation of the perturbative series reads

$$\begin{aligned} \delta_{S,CI}^{(2-\text{mass})} &= -8\frac{m_s^2(M_\tau^2)}{M_\tau^2} \\ &\times[0.97+0.49+0.38+(0.34\pm0.04)]\,, \end{aligned} \tag{41}$$

with somewhat improved convergence compared to FOPT (40). Therefore, the results of the following analysis are based on the FOPT_{CI} approach.

Independently of whether FOPT or FOPT_{CI} is used, the origin of the convergence problem is found in the $J = 0$ component as defined in (37)

$$\begin{aligned} \delta_S^{(2-\text{mass})}(J=0) &= -8\frac{m_s^2(M_\tau^2)}{M_\tau^2} \\ &\times[0.41+0.32+0.32+0.37]\,, \end{aligned} \tag{42}$$

while the $J = 1+0$ part converges very well,

$$\begin{aligned} &\delta_S^{(2-\text{mass})}(J=1+0) \\ &= -8\frac{m_s^2(M_\tau^2)}{M_\tau^2}\,[0.56+0.16+0.05-(0.04\pm0.04)]\,. \end{aligned} \tag{43}$$

Following these observations, two methods are considered in the following in order to determine $m_s(M_\tau^2)$:

- in the *inclusive method*, the inclusive strange hadronic rate is considered and both $J = 1+0$ and $J = 0$ are included with their respective convergence behaviour taken into account in the theoretical uncertainties.
- the *'1+0' method* singles out the well-behaved $J = 1+0$ part by subtracting the experimentally determined $J = 0$ longitudinal component from data. The measurement is then less inclusive and the sensitivity to m_s is significantly reduced; however, the δ_2 perturbative expansion is under control and the corresponding theoretical uncertainty is reduced.

Since the $J = 0$ expansion is problematic, the results are given with the '1+0' method, while the inclusive approach is used as an insight into the handling of (42).

7.1.2 Nonperturbative contributions

The last term in (38) represents the nonperturbative contribution which, using the OPE, can be written as a sum of powers of M_τ^D:

$$\delta^{(D)} = \sum_{\dim\mathcal{O}=D} C(s,\mu)\frac{\langle\mathcal{O}(\mu)\rangle}{(-M_\tau^2)^{D/2}} , \qquad (44)$$

where the parameter μ separates the long-distance nonperturbative effects, absorbed into the vacuum expectation elements $\langle\mathcal{O}(\mu)\rangle$, from the short-distance effects which are included in the Wilson coefficients $C(s,\mu)$ [47].

The dimension $D = 4$ operators have dynamical contributions from the gluon condensate $\langle(\alpha_s/\pi)GG\rangle$, the quark condensates $m_u\langle\bar{u}u\rangle$, $m_d\langle\bar{d}d\rangle$ and $m_s\langle\bar{s}s\rangle$, and the running quark masses to the fourth power. The contributions from dimension $D = 6$ and $D = 8$ operators are rather complex and they are taken into account by introducing effective scale independent operators $\langle\mathcal{O}_6\rangle$ and $\langle\mathcal{O}_8\rangle$ that are fitted to the data.

7.2 Evidence for the effect of a massive strange quark

From the result found from this analysis on the branching ratio for τ decays into all strange hadronic final states (27), one obtains

$$R_{\tau,S} = 0.1610 \pm 0.0066 , \qquad (45)$$

using the value for $B(\tau^- \to e^-\bar{\nu}_e\nu_\tau)$ given in Sect. 6.

The result (45) can be readily compared with the QCD prediction for a massless strange quark neglecting the nonperturbative contributions,

$$R_{\tau,S}^{(0)} = 0.1809 \pm 0.0036 , \qquad (46)$$

where the quoted error mainly reflects the uncertainties on $\alpha_s(M_\tau^2)$ and V_{us}. The two values differ by 2.7σ, in the direction predicted for a non-zero m_s value.

This is evidence for the effect of a massive strange quark in a single observable which is essentially predicted by perturbative QCD, providing the basis for the determination of the running mass m_s at the scale of the τ mass.

7.3 Spectral moments

As proposed in [48] and successfully applied in several $\alpha_s(M_\tau^2)$ analyses [2,49–51], the spectral functions are used to construct the moments

$$R_{\tau,(S)}^{kl} \equiv \int_0^{M_\tau^2} ds \left(1-\frac{s}{M_\tau^2}\right)^k \left(\frac{s}{M_\tau^2}\right)^l \frac{dR_{\tau,(S)}}{ds} , \qquad (47)$$

with $R_{\tau,(S)}^{00} = R_{\tau,(S)}$ for the nonstrange and the strange cases, respectively. The theoretical prediction for the moments (47) follows the line described above, leading to expressions similar to (38) with nonperturbative contributions $\delta^{kl(D)}$ [15]. Fitting the τ decay rate and the spectral moments allows $m_s(M_\tau^2)$ and the nonperturbative operators of dimension $D = 6$ and $D = 8$ to be simultaneously obtained.

In order to reduce the theoretical uncertainties, the difference between nonstrange and strange spectral moments, properly normalized with their respective CKM matrix elements, is considered:

$$\Delta_\tau^{kl} \equiv \frac{1}{|V_{ud}|^2}R_{\tau,S=0}^{kl} - \frac{1}{|V_{us}|^2}R_{\tau,S=-1}^{kl} , \qquad (48)$$

for which the massless perturbative contribution vanishes so that the theoretical prediction now reads (setting $m_u = m_d = 0$)

$$\Delta_\tau^{kl} = 3S_{\rm EW}\left(-\delta_S^{kl(2-{\rm mass})} + \sum_{D=4,6,\ldots}\tilde{\delta}^{kl(D)}\right) . \qquad (49)$$

For the dimension $D = 4$ nonperturbative contribution, the flavour independent gluon condensate disappears in the difference, leaving only the quark condensate terms. The fitted $\tilde{\delta}^{kl(6,8)}$ contain the higher-order nonperturbative contributions to the difference of nonstrange and strange moments. Since the nonstrange nonperturbative contributions to the inclusive $V + A$ hadronic decay ratio have been found to be very small [2], one has $\tilde{\delta}^{kl(4,6,8)} \approx -\delta_S^{kl(4,6,8)}$.

In this analysis, the nonstrange spectral function obtained from [2] has been appropriately scaled making use of the updated value of $R_{\tau,S}$.[4] The experimental results of the spectral moments (48) and their correlations are given in Table 8. For the CKM matrix elements the values $|V_{ud}| = 0.9751\pm0.0004$ and $|V_{us}| = 0.2218\pm0.0016$ [18] are used, while the errors are included in the theoretical uncertainties discussed in the next section. In the inclusive $V + A$ nonstrange case the correlations between the hadronic decay ratio, obtained essentially using universality from the leptonic branching ratios and the τ lifetime, and the spectral moments are negligible (see [2]). On the contrary, all (k,l) moments used here suffer from large correlations due to the common input from the strange spectral function. This reduces the independent information used in the fit and thus generates strong correlations between the adjusted parameters.

Figure 10 shows the weighted integrand of the lowest moment Δ_τ^{00} (see (47),(48)) from the ALEPH data, as a function of the invariant mass-squared, and for which the expectation from massless perturbative QCD vanishes.

[4] $R_{\tau,S=0}$ is obtained from the difference $R_\tau - R_{\tau,S}$, in which R_τ is directly derived from the leptonic branching ratio quoted in Sect. 6

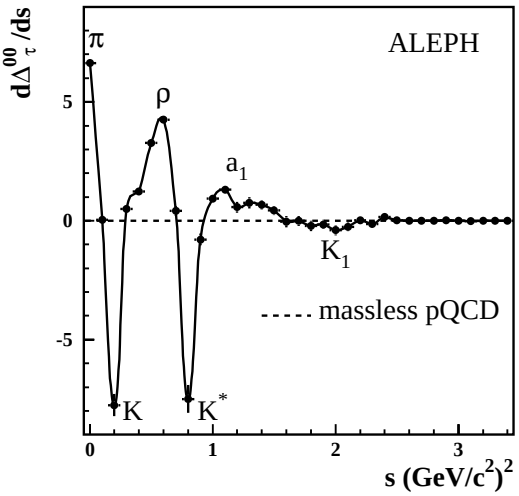

Fig. 10. Integrand of (48) for (k=0, l=0), *i.e.*, difference of the Cabibbo corrected nonstrange and strange invariant mass spectra. The contribution from massless perturbative QCD vanishes in the difference

Table 8. Measured spectral moments Δ_τ^{kl} (left table) and their experimental correlations (right table)

(k,l)	Δ_τ^{kl}
(0,0)	0.394 ± 0.137
(1,0)	0.383 ± 0.078
(2,0)	0.373 ± 0.054
(1,1)	0.010 ± 0.029
(1,2)	0.006 ± 0.015

(k,l)	(0,0)	(1,0)	(2,0)	(1,1)	(1,2)
(0,0)	1	0.94	0.83	0.98	0.91
(1,0)	–	1	0.97	0.87	0.72
(2,0)	–	–	1	0.72	0.53
(1,1)	–	–	–	1	0.95
(1,2)	–	–	–	–	1

7.4 Separation of $J = 0, 1$ components

Although the $J = 0$ component has not been thoroughly investigated in the data, it is clear that it is dominated by the single K pole. Other contributions can be identified: *(i)* off-shell vector K^* resonances can generate a 0^+ component [52], however too small to have a significant effect in this analysis, and *(ii)* production of the scalar $K_0^*(1430)$ resonance may occur as discussed below.

The $K_0^*(1430)$ state decays almost exclusively into $K\pi$ with a branching ratio of $(93 \pm 10)\%$ [18] and a fit to the $K^-\pi^0$ mass distribution as discussed in Sect. 4.1 provides a branching ratio $B(\tau \to K_0^*(1430)\nu_\tau) = (0.0 \pm 2.5) \times 10^{-4}$. It is therefore clear that 0^+ contributions are strongly suppressed ($< 1.6 \times 10^{-2}$) compared to the dominant 1^- production. This is expected from chiral symmetry breaking, with contributions reduced by $\sim (m_K/M_\tau)^4$ as discussed in [52], not including the τ kinematic factor which disfavours higher mass states.

No direct estimate of extra 0^- components beyond the single K can be made from the present data in the $\overline{K}\pi\pi$ modes. This is due to the lack of statistics and to the background subtraction, especially in the high mass region where some evidence for a broad pseudoscalar state at 1460 MeV/c^2 exists [18]. A contribution equal to the 0^+ one (actually an upper limit) is assumed in this case.

The evaluation of the $J = 0$ contributions to $R_{\tau,S}$ obtained from integration of (37) using f_K from (6) gives

$$R_{\tau,S}^{(0)}(K) = -0.00615 \pm 0.00026 \ , \quad (50)$$

$$R_{\tau,S}^{(0)}(\text{other } 0^-, 0^+) = -0.0015 \pm 0.0015 \ , \quad (51)$$

leading to the result

$$\Delta_\tau^{00}(J = 0) = 0.155 \pm 0.031 \ , \quad (52)$$

where the $J = 0$ contributions in the nonstrange part have been computed to be -0.00076 for the π pole (using the corresponding ALEPH branching ratio [31]) and safely assumed to be negligible in the other modes. Similarly, the $J = 0$ contributions are obtained for all (k, l) values and subtracted from the measured moments.

7.5 Theoretical parameters and uncertainties

The recent ALEPH measurement of the strong coupling constant [2], $\alpha_s(M_\tau^2) = 0.334 \pm 0.007_{\rm exp} \pm 0.021_{\rm th}$, is used. The theoretical error is dominated by uncertainties due to the truncation of the perturbative series so that correlations between the above value and the moments (48) are negligible, with the latter dominated by the uncertainties on the strange part.

The dependence on the renormalization scheme ($\overline{\rm MS}$) used is already included in the theoretical error on $\alpha_s(M_\tau^2)$ and thus not further added in order to avoid double counting.

The renormalization scale (μ) dependence of the $D = 2$ prediction has been studied in [13]. When varying μ away from M_τ, additional logarithms enter the series and due to its truncation at finite order, a residual dependence on μ is left. To estimate the associated uncertainty, μ is varied from 1.3 to 3.6 GeV/c^2.

The uncertainty originating from the truncation of the perturbative series for the dimension $D = 2$ term is handled as follows: the estimated error is taken as the full size of the last term retained in the expansion, namely of order α_s^3 for the $J = 1 + 0$ series. Some redundancy is expected between the uncertainties estimated for the renormalization scale dependence and the truncation of the perturbative series. However, both errors are conservatively kept and added in quadrature.

For the dimension $D = 4$ nonperturbative contribution the products of quark condensates and quark masses are taken from the PCAC relations with some correction for the strange quark [15]. No errors are introduced for the higher dimensional operators since they are fixed experimentally. Finally, a small uncertainty is included from the error on $S_{\rm EW}$.

Table 9 gives the above theoretical uncertainties on $m_s(M_\tau^2)$. The main error contribution stems from the $|V_{us}|$ uncertainty [18].

7.6 Results

The fit minimizes the χ^2 of the differences between measured and fitted quantities contracted with the inverse of

Table 9. Theoretical uncertainties on $m_s(M_\tau^2)$. The uncertainty from the truncation of the perturbative series for the $D = 2$ mass term is estimated from adding or subtracting the value of the last retained term in the QCD expansion. The unequal positive and negative errors on m_s are averaged

Error source	Range	$\Delta m_s(M_\tau^2)$ (MeV/c^2)
$\alpha_s(M_\tau^2)$	0.334 ± 0.022	3
truncation		11
R-scale μ	$(1.3 - 3.6)$ GeV/c^2	6
$m_s\langle\bar{s}s\rangle$	$-(1.63 \pm 0.29) \times 10^{-3}$ GeV^4	1
$S_{\rm EW}$	1.0194 ± 0.0040	1
$\lvert V_{us}\rvert$	0.2218 ± 0.0016	22
Total errors		26

the sum of the experimental and theoretical covariance matrices. Due to the large correlations and the statistical limitation of the spectral functions at the end of the τ phase space, higher moments $l > 2$ do not add significant information to the fit. The results for $m_s(M_\tau^2)$ and the nonperturbative contributions to $\Delta_\tau^{00(1+0)}$ for the '1+0' method are

$$m_s(M_\tau^2) = \left(176\,^{+37_{\rm exp}+24_{\rm th}}_{-48_{\rm exp}-28_{\rm th}} \pm 8_{\rm fit} \pm 11_{J=0}\right)\ {\rm MeV}/c^2\ , \quad (53)$$

$$\tilde{\delta}^{(6)} = 0.039 \pm 0.016_{\rm exp} \pm 0.014_{\rm th} \pm 0.004_{\rm fit}\ , \quad (54)$$

$$\tilde{\delta}^{(8)} = -0.021 \pm 0.014_{\rm exp} \pm 0.008_{\rm th} \pm 0.003_{\rm fit}\ , \quad (55)$$

with a χ^2/ndf of 0.2/2.

The errors are separated according to their experimental, theoretical, fit and spin separation origins. The fit error stems from an intrinsic bias in the χ^2 minimization, due to the large correlations of the input observables, and includes the total difference between the fit results with and without correlations, while the results without correlations are given as central values, as discussed in [53]. The correlation matrix corresponding to the fit results is given in Table 10.

The result (53)

$$m_s(M_\tau^2) = (176\,^{+46}_{-57})\ {\rm MeV}/c^2 \quad (56)$$

can be evolved to the scale of 1 GeV using the four-loop RGE γ-function [46], yielding

$$m_s(1\ {\rm GeV}^2) = (234\,^{+61}_{-76})\ {\rm MeV}/c^2\ . \quad (57)$$

The fitted m_s value corresponds to a contribution $\delta_S^{(2)} = -(0.058 \pm 0.027)$ to $R_{\tau,S}^{(1+0)}$. No operator of dimension $D = 4$ has been fitted except the small quartic strange mass corrections, for a total contribution $\delta_S^{(4)} = -(0.003 \pm 0.001)$, dominated by the strange quark condensate; the error given is almost entirely of theoretical origin. The $D = 6$ and $D = 8$ strange contributions are $\delta_S^{(6)} = -0.038 \pm 0.022$ and $\delta_S^{(8)} = 0.020 \pm 0.016$. They are fairly large compared to the nonstrange case, $\delta^{(6)} = 0.001 \pm 0.004$ and $\delta^{(8)} = -0.001 \pm 0.001$ [2].

Table 10. Correlation matrix according to the '1+0' fit results

	$m_s(M_\tau^2)$	$\tilde{\delta}^{(6)}$	$\tilde{\delta}^{(8)}$
$m_s(M_\tau^2)$	1	0.74	−0.92
$\tilde{\delta}^{(6)}$	–	1	−0.83
$\tilde{\delta}^{(8)}$	–	–	1

The above results are obtained from the $J = 1 + 0$ piece which was shown in Sect. 7.1.1 to have a satisfactory convergence in QCD. The inclusive method has a better experimental definition, but suffers from the bad convergence properties of the $J = 0$ part for which a prescription must be specified. A reasonable rule to handle an asymptotic series is to truncate it where the terms reach a minimum and then assign as an uncertainty the full amount of the last term retained. With this prescription, the $J = 0$ expansion is stopped after the $O(\alpha_s)$ term and, going through the same steps as before, one gets

$$m_s(M_\tau^2) = (149\,^{+24_{\rm exp}+21_{\rm th}}_{-30_{\rm exp}-25_{\rm th}} \pm 6_{\rm fit})\ {\rm MeV}/c^2\ , \quad (58)$$

where this time the theoretical uncertainty is dominated by the truncation of the perturbative series. The fitted nonperturbative parts are $\tilde{\delta}^{(6)} = 0.031 \pm 0.015$ and $\tilde{\delta}^{(8)} = -0.018 \pm 0.011$. The results (53) and (58) are consistent within the uncorrelated part of their errors with a χ^2/ndf of 1.4/1.

It may be interesting to come back to the discarded $J = 0$ part in order to get some information regarding the handling of its ill-behaved perturbative expansion, (43). Truncating the series at the minimum provides a result consistent with (53), while keeping the two more known terms destroys the consistency. This observation supports the prescription used in the inclusive method. However, as stated above, the safer determination with the '1+0' method is preferred and given as the final result of this analysis.

As shown for the nonstrange case in [2], one can simulate the physics of a hypothetical τ lepton with mass $\sqrt{s_0}$ smaller than M_τ by replacing M_τ^2 everywhere in (37) by s_0. Under the assumption of quark-hadron duality, the evaluation of the observables as a function of s_0 constitutes a test of the OPE approach adopted here, since the energy dependence of the theoretical predictions is determined once the parameters are fixed. Figure 11 shows the running observable $\Delta_\tau^{00(1+0)}(s_0)$ compared to the corresponding theoretical predictions and the fitted parameters in (53,54,55). Despite the expected breakdown of the perturbative approach at lower scales, it is noteworthy that the prediction agrees with data at such a low mass scale within the theoretical uncertainties used in the analysis.

7.7 Comparison with other determinations of m_s

Other determinations of m_s have been obtained by analyses of the divergence of the vector and axial-vector current two-point function correlators [54–64]. The phenomenological information on the associated scalar and pseudoscalar spectral functions is reconstructed from phase-shift resonance analyses which are yet incomplete over the considered mass range and need to be supplemented by other assumed ingredients, in particular the description of the continuum, thus introducing systematic effects.

Another approach [65] considers the difference between isovector and hypercharge vector current correlators as related to the $I = 1$ and $I = 0$ spectral functions accessible in e^+e^- annihilation into hadrons at low energy. A recent reanalysis [66] points out the possibility of large corrections from isospin breaking, leading to significant deviations for the extracted m_s value.

Finally, lattice QCD calculations of m_s are available [67–70]. Their values show quite a large spread.

The present determination of m_s is directly compared with the other derivations in Fig. 12 where all values are given at a mass scale of 1 GeV. Qualitative agreement is observed, the value from the present analysis being rather on the high side of the range of previous determinations. The precision of the result is unfortunately still limited. As an example, the Standard Model prediction for the CP-violation parameter ϵ'/ϵ is strongly dependent on the value of m_s and the present determination translates into a range of ϵ'/ϵ values spanning a factor of five [9], but favouring "low" values for this ratio.

8 Conclusion

All ALEPH measurements on τ decays with kaons are summarized to provide an overall review and a comprehensive study of these decays.

Comparing the decays $\tau^- \to K^-\nu_\tau$ and $K^- \to \mu^-\nu_\tau$ shows agreement with $\mu-\tau$ universality within 2% uncertainty.

The investigation of mass spectra shows that the $(\overline{K}\pi)^-$ decay mode is dominated by $K^*(892)^-$. A $K^*(1410)$ contribution is extracted from a fit to the $\overline{K}\pi$ mass spectrum through its interference with the dominant $K^*(892)$.

The $(\overline{K}\pi\pi)^-$ decay modes are observed to proceed through the $K_1(1270)$, $K_1(1400)$ and $K^*(1410)$ resonances. The relative contributions are extracted by fitting the $\pi\pi$ and $\overline{K}\pi\pi$ mass spectra, separating the vector and axial-vector contributions. The vector current contribution to the $\overline{K}\pi\pi$ modes is found to be $(23^{+22}_{-17})\%$.

According to CVC, the vector spectral function for the $(K\overline{K}\pi)^-$ modes is connected to low energy e^+e^- annihilation, allowing one to conclude that $(94^{+6}_{-8})\%$ of this decay mode proceeds through the axial-vector current. Because the latter is dominated by the a_1 resonance, a branching ratio $B(a_1 \to K^*K) = (2.6 \pm 0.3)\%$ is obtained.

Tests of isospin symmetry for the $(\overline{K}\pi)^-$, $(\overline{K}\pi\pi)^-$ and $(K\overline{K}\pi)^-$ modes are performed. A good consistency with the expectation from isospin invariance is observed, providing useful information on the decay dynamics in these final states.

The branching ratio for τ decay into all strange final states is determined to be $B(\tau^- \to X^-(S = -1)\nu_\tau) = (28.7 \pm 1.2) \times 10^{-3}$ and the total strange spectral function is derived from the corresponding mass spectra.

Using the total rates, as well as moments of the respective spectral functions, through a combination of strange and nonstrange parts which cancel the dominant massless perturbative QCD contribution, a global fit is performed providing a determination of the strange nonperturbative

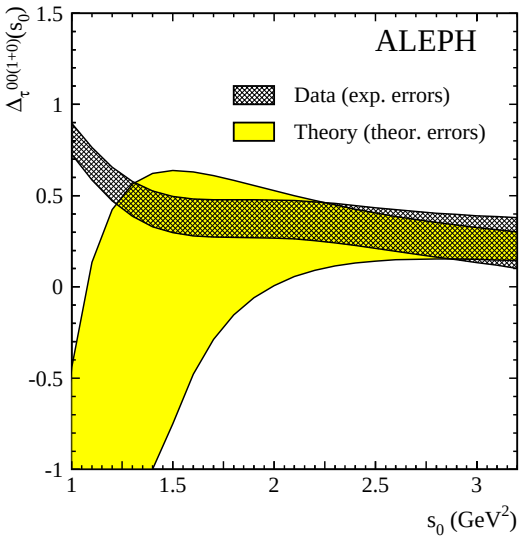

Fig. 11. The observable $\Delta_\tau^{00(1+0)}(s_0)$ as a function of the "τ-mass"-squared s_0. The curve is plotted as a one-standard deviation error band to emphasize its strong point-to-point correlations. Also shown is the theoretical prediction for the fit parameters given in (53,54,55)

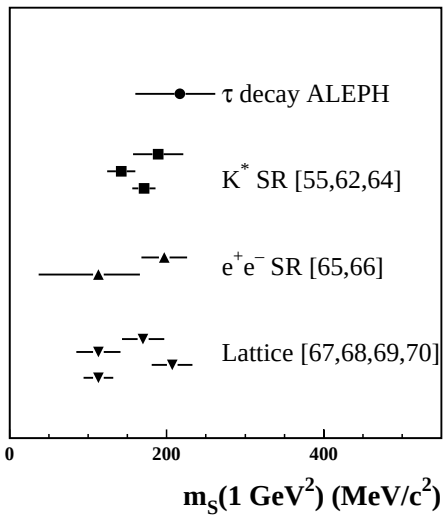

Fig. 12. The ALEPH determination of $m_s(1\ \mathrm{GeV}^2)$ compared to the results of other approaches. Details are given in the text (SR = sum rules). The references are listed in the order of the results from top to bottom

contributions and of the s quark mass. The value obtained is $m_s(M_\tau^2) = (176^{+46}_{-57})$ MeV/c^2, which is evolved to 1 GeV to yield $m_s(1\ \mathrm{GeV}^2) = (234^{+61}_{-76})$ MeV/c^2, in agreement with other determinations.

Acknowledgements. We are indebted to K.G. Chetyrkin, J.H. Kühn, K. Maltman, A. Pich and J. Prades for useful discussions. We also wish to thank our colleagues in the CERN accelerator divisions for the successful operation of the LEP storage ring. We thank the engineers and technicians in all our institutions for their support in constructing and operating ALEPH. Those of us from nonmember states thank CERN for its hospitality.

References

1. ALEPH Collaboration, *Measurement of the spectral functions of vector current hadronic τ decays*, Z. Phys. **C76** (1997) 15.
2. ALEPH Collaboration, *Measurement of the spectral functions of axial-vector hadronic τ decays and determination of $\alpha_S(\mathrm{M}_\tau^2)$*, Eur. Phys. J. **C4** (1998) 409.
3. M. Davier, Nucl. Phys. **B** (Proc. Suppl.) **55** (1997) 395; S.M. Chen, Nucl. Phys. **B** (Proc. Suppl.) **64** (1998) 265.
4. S.M. Chen, M. Davier and A. Höcker, Nucl. Phys. **B** (Proc. Suppl.) **76** (1999) 369.
5. ALEPH Collaboration, *Three-prong τ decays with charged kaons*, Eur. Phys. J. **C1** (1998) 65.
6. ALEPH Collaboration, *K_S^0 production in τ decays*, Eur. Phys. J. **C4** (1998) 29.
7. ALEPH Collaboration, *One-prong τ decays with kaons*, Eur. Phys. J. **C10** (1999) 1.
8. ALEPH Collaboration, *A study of τ decays involving η and ω mesons*, Z. Phys. **C74** (1997) 263.
9. A. Buras et al., Phys. Lett. **B389** (1996) 749.
10. E. Braaten, S. Narison and A. Pich, Nucl. Phys. **B373** (1992) 581.
11. K.G. Chetyrkin and A. Kwiatkowski, Z. Phys. **C59** (1993) 525.
12. K. Maltman, *Problems With Extracting m_s from Flavour Breaking in Hadronic τ Decays*, Phys. Rev. **D58** (1998) 093015
13. A. Pich and J. Prades, *Perturbative Quark Mass Corrections to the Tau Hadronic Width*, JHEP 9806 (1998) 13.
14. K.G. Chetyrkin, J.H. Kühn and A.A. Pivovarov, *Determining the Strange Quark Mass in Cabibbo Suppressed Tau Lepton Decays*, Nucl. Phys. **B533** (1998) 473.
15. S.M. Chen, M. Davier and A. Höcker, *Determination of m_s from strange τ decays*, LAL 98-90 (November 1998).
16. L. Rolandi, Nucl. Phys. **C** (Proc. Suppl.) **55** (1997) 461.
17. R. Decker and M. Finkemeier, Phys. Lett. **B334** (1994) 199; Nucl. Phys. **B438** (1995) 17.
18. R.M. Barnett et al., Particle Data Group, Phys. Rev. **B54** (1996) 1.
19. H.B. Thacker and J.J. Sakurai, Phys. Lett. **B36** (1971) 103.
20. M. Finkemeier, E. Mirkes, Z. Phys. **C69** (1996) 243.
21. R.K. Carnegie et al., Nucl. Phys, **B127** (1977) 509; Phys. Lett. **B68** (1977) 287.
22. C. Daum et al., ACCMOR Collaboration, Nucl. Phys. **B187** (1981) 1.
23. R. Decker et al., Z. Phys. **C58** (1993) 445.
24. F.J. Gilman and S.H. Rhie, Phys. Rev. **D31** (1985) 1066.
25. A. Rougé, Z. Phys. **C70** (1996) 65.
26. A. Rougé, Eur. Phys. J. **C4** (1998) 265.
27. T.E. Coan et al., CLEO Collaboration, Phys. Rev. **D53** (1996) 6037; J.M. Yelton et al., MARKII Collaboration, Phys. Rev. Lett. **56** (1986) 812; H. Aihara et al., TPC Collaboration, Phys. Rev. Lett. **59** (1987) 751; R. Tschirhart et al., HRS Collaboration, Phys. Lett. **B205** (1988) 407; H. Albrecht et al., ARGUS Collaboration, Z. Phys. **C41** (1988) 1; M. Acciarri et al., L3 Collaboration, Phys. Lett. **B352** (1995) 487.
28. A. Pais, Ann. Phys. **9** (1960) 548; **22** (1963) 274.
29. F. Mane et al., DM1 Collaboration, Phys. Lett. **112B** (1982) 178.
30. D. Bisello et al., DM2 Collaboration, Z. Phys. **C52** (1991) 227.
31. ALEPH Collaboration, *τ hadronic branching ratios*, Z. Phys. **C70** (1996) 579.
32. D.M. Asner et al., CLEO Collaboration, CLNS-99-1601, hep-ex/9902022.
33. J.J. Gomez-Cadenas et al., Phys. Rev. **D42** (1990) 3093.
34. B.A. Li, Phys. Rev. **D55** (1997) 1436.
35. Yung-Su Tsai, Phys. Rev. **D4** (1971) 2822.
36. J.Z. Bai et al., BES Collaboration, Phys. Rev. **D53** (1996) 20.
37. W. Marciano and A. Sirlin, Phys. Rev. Lett. **56** (1986) 22.
38. M.A. Shifman, A.L. Vainshtein and V.I. Zakharov, Nucl. Phys. **B147** (1979) 385, 448, 519.
39. E. Braaten and C.S. Li, Phys. Rev. **D42** (1990) 3888.
40. L.R. Surguladze and M.A. Samuel, Phys. Rev. Lett. **66** (1991) 560; S.G. Gorishny, A.L. Kataev and S.A. Larin, Phys. Lett. **B259** (1991) 144.
41. K.G. Chetyrkin, Phys. Lett. **B390** (1997) 309.
42. K.G. Chetyrkin and J. Kühn, Phys. Lett. **B406** (1997) 102.
43. F. Le Diberder and A. Pich, Phys. Lett. **B286** (1992) 147.
44. A.A. Pivovarov, Sov. J. Nucl. Phys. **54** (1991) 676; Z. Phys. **C53** (1992) 461.
45. S.A. Larin, T. van Ritbergen and J.A.M. Vermaseren, Phys. Lett. **B400** (1997) 379.
46. S.A. Larin, T. van Ritbergen and J.A.M. Vermaseren, Phys. Lett. **B405** (1997) 327.
47. K.G. Wilson, Phys. Rev. **179** (1969) 1499.
48. F. Le Diberder and A. Pich, Phys. Lett. **B289** (1992) 165.
49. ALEPH Collaboration, *Measurement of the strong coupling constant using τ decays*, Phys. Lett. **B307** (1993) 209.
50. T.E. Coan et al., CLEO Collaboration, Phys. Lett. **B356** (1995) 580.
51. K. Ackerstaff et al., OPAL Collaboration, Eur. Phys. J. **C7** (1999) 571.
52. M. Finkemeier and E. Mirkes, Z. Phys. **C72** (1996) 619.
53. G. D'Agostini, Nucl. Inst. Meth. **A346** (1994) 306.
54. J. Gasser and H. Leutwyler, Phys. Rep. **87** (1982) 77.
55. M. Jamin and M. Münz, Z. Phys. **C66** (1995) 633.
56. K.G. Chetyrkin et al., Phys. Lett. **B404** (1997) 337.
57. C. Becchi et al., Z. Phys. **C8** (1981) 335.
58. C.A. Dominguez and E. de Rafael, Ann. Phys. **174** (1987) 372.
59. C.A. Dominguez et al., Phys. Lett. **B253** (1991) 241.
60. M. Jamin, Nucl. Phys. **B** (Proc. Suppl.) **64** (1998) 250.
61. A.L. Kataev et al., Nuovo. Cim. **A76** (1983) 723.

62. P. Colangelo et al., Phys. Lett. **B408** (1997) 340.
63. S. Narison, Phys. Lett. **B216** (1989) 191.
64. K.G. Chetyrkin et al., Phys. Rev. **D51** (1995) 5090.
65. S. Narison, Phys. Lett. **B358** (1995) 113.
66. K. Maltman, Phys. Lett. **B428** (1998) 179.
67. C.R. Allton et al., Nucl. Phys. **B431** (1994) 667.
68. R. Gupta and T. Bhattacharya, Phys. Rev. **D55** (1997) 7203.
69. N. Eicker et al., SESAM-Collaboration, hep-lat/9704019.
70. B.J. Gough et al., Phys. Rev. Lett. **79** (1994) 1662.